Propagation of periodic patterns in a discrete system with competing interactions

Anna Vainchtein[†], Erik S. Van Vleck[‡], and Aijun Zhang[§]

Abstract. In this paper we consider bistable lattice differential equation with competing first and second nearest neighbor interactions. We construct heteroclinic orbits connecting the stable zero equilibrium state with stable spatially periodic orbits of period $p = 2, 3, 4$ using transform techniques and a bilinear bistable nonlinearity. We investigate the existence, global structure, and multiplicity of such traveling wave solutions. We show that in a certain parameter range the $p = 2$ patterns have a finite maximum propagation speed. Our analysis also shows that multiple solutions involving a $p = 4$ pattern may coexist at some velocities. Numerical simulations suggest stability of some of the obtained solutions.

Key words. Periodic patterns, lattice differential equation, competing interactions, traveling wave solution

AMS subject classifications. 34K31, 37L60

1. Introduction. Many physical and biological systems with an underlying spatially discrete structure may be effectively modeled using lattice differential equations. For example, bistable systems such as the discrete Nagumo equation have been employed to model propagation of action potentials in myelinated nerve fibers [21], and monostable systems involving discrete KPP-Fisher equations are used to model the spread of populations in patchy environments [18]. In addition, there are many examples in fluid dynamics and neurophysiology (see, for example, [3, 15, 23] and the references therein). Lattice models are also widely used in physics and materials science to describe crack propagation, friction, charge-density waves, motion of domain walls, phase boundaries and dislocations, solitary waves, discrete breathers and many other phenomena where spatial discreteness plays an important role [5, 9, 12, 22, 27, 30].

The interplay between different interactions in a spatially discrete system often leads to formation of periodic patterns. Examples include twinning microstructures in shape memory alloys [4], domain-wall microstructures in dielectric crystals [28] and patterns in neural networks [14]. Dynamics of these patterns is an interesting and relatively unexplored topic.

In this paper we consider a prototypical spatially discrete dynamical system that describes formation and propagation of periodic patterns. The system corresponds to the overdamped Frenkel-Kontorova model [5] with bistable onsite nonlinearity and harmonic interactions and is governed by the dimensionless equations

$$\dot{y}_n(t) = d_1(y_{n+1} - 2y_n + y_{n-1}) + d_2(y_{n+2} - 2y_n + y_{n-2}) - f(y_n). \tag{1.1}$$

[†]Department of Mathematics, University of Pittsburgh, Pittsburgh, PA 15260, aav4@pitt.edu. This author's work was supported by NSF grant DMS-1007908.
[‡]Department of Mathematics, University of Kansas, Lawrence, KS 66045, evanvv@ku.edu. This author's work was supported by NSF grants DMS-1115408 and DMS-1419047.
[§]Department of Mathematics, Drexel University, Philadelphia, PA 19104, az372@drexel.edu

Here $y_n(t)$ is the displacement of nth particle, $\dot{y}_n(t) = y'_n(t)$, d_1 and d_2 denote the elastic moduli of the harmonic interactions between first and second neighbors, respectively, and $f(y_n)$ is a bistable nonlinear interaction force due to an onsite potential. To obtain analytical results, we consider a bilinear form of the bistable nonlinearity:

$$(1.2) \qquad\qquad f(u) = u - \theta(u - a), \quad a > 0,$$

where $\theta(x)$ is the unit step function and a is the detuning parameter.

As in section 3 of [8] we regard f as set valued when $u = a$, i.e.,

$$f(a) = [a - 1, a], \ \ \theta(0) = [0, 1],$$

but otherwise f and θ are single-valued. By a solution we mean $y(t) \in l^\infty(\mathbb{Z})$ for which each coordinate function $y_n(t)$ is absolutely continuous and satisfies the differential inclusion

$$(1.3) \qquad \dot{y}_n(t) \in d_1(y_{n+1} - 2y_n + y_{n-1}) + d_2(y_{n+2} - 2y_n + y_{n-2}) - f(y_n)$$

for almost every t. The solution has jump discontinuities in the first derivative when $y_n(t) = a$, but elsewhere the solution is C^1 and (1.1) holds in the classical sense. In particular, the existence and uniqueness theory of Filippov systems [17] applies directly when a coordinate crosses the discontinuity surface $u = a$ transversally.

Observe that under these assumptions the system (1.1) always has a (trivial) equilibrium solution $y_n \equiv 0$, and that $y_n \equiv 1$ is also an equilibrium state when $a < 1$. Traveling wave connecting the homogeneous states have been extensively studied for the bistable lattice Nagumo equation ($d_1 > 0$, $d_2 = 0$) [8, 16, 21, 23], and the existence of such waves in the more general case with long-range interactions was proved in [2], under the assumption that in this setting corresponds to $d_1 + 4d_2 > 0$.

When the parameters d_1, d_2 and a take values within certain regions, the system also has stable periodic equilibrium states that correspond to various microstructural patterns, due to the competition between the linear interactions and the nonlinear term. In this work we are interested in dynamic solutions that describe steady propagation of such patterns in the lattice. To illustrate the existence of such solutions, we conducted numerical simulations of (1.1) with (1.2) on a finite lattice of 408 particles with free boundary conditions and initial conditions shown in Fig. 1a, with several particles in the middle displaced slightly above or slightly below a, while the other particles have zero displacement. Here and in what follows, the default multistep numerical method (either Adams predictor-corrector method or, for stiff systems, Gear's method) with adaptive step size in NDSolve in Mathematica was used in numerical simulations. These are higher order convergent methods with local error estimation and step size selection that are appropriate for the type of differential equations considered in this paper. Numerical solution of the initial value problem features formation and steady growth of a symmetric microstructural pattern, a snapshot of which is depicted in Fig. 1b. In the enlarged view of the right front shown in Fig. 1c one can see a periodic state of the period $p = 5$ propagating to the right into the zero state. As the parameters are varied, other periodic patterns can be generated. For example, Fig. 2 shows patterns with $p = 4$ (top left), $p = 2$ (top right), $p = 3$ (bottom right) and $p = 13$ (bottom left).
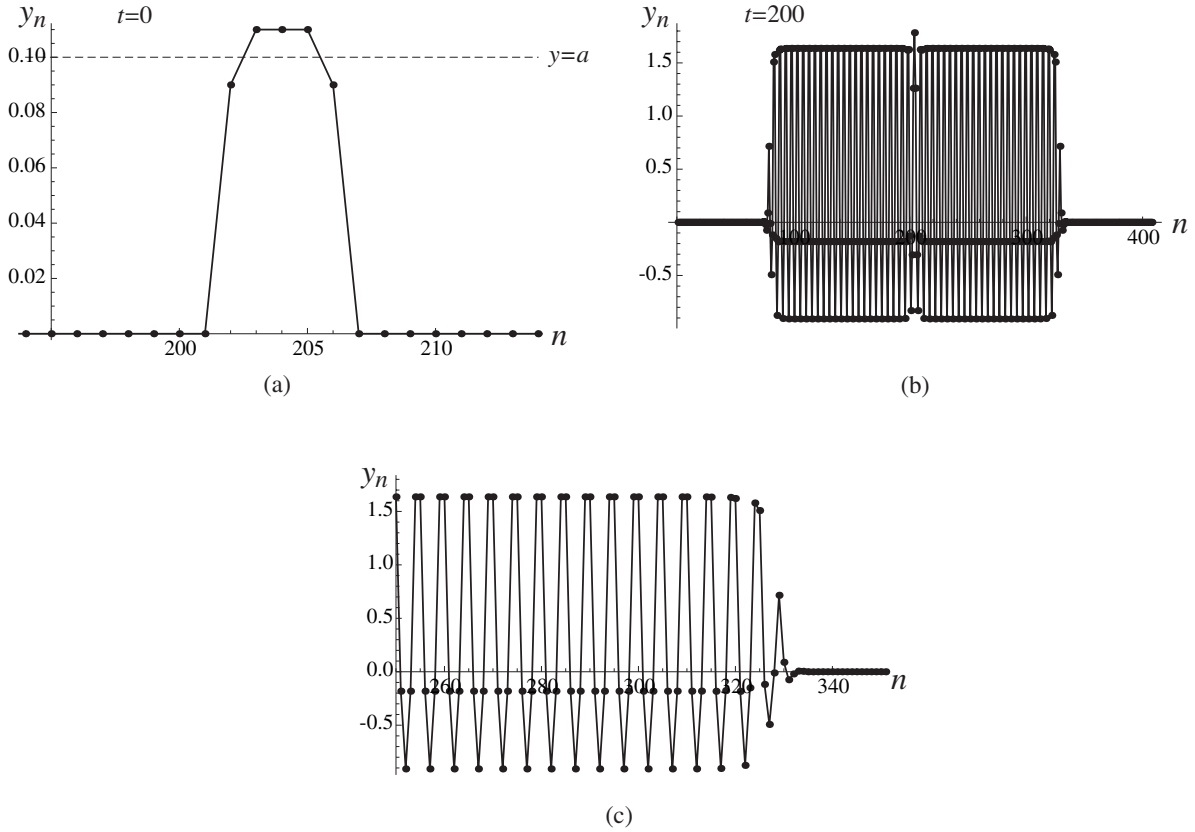
Figure 1. *(a) Initial condition for numerical simulation results shown in this figure and Fig. 2. (b) Snapshot of solution of* (1.1) *with* (1.2) *at* $d_1 = 0.25$, $d_2 = -0.25$, $a = 0.1$, $t = 200$ *with initial condition in (a). (c) Enlarged view of the right front of the solution in (b).*

Physical motivation for (1.1) appears in [31], where a model for phase transitions is considered that consists of a chain of particles, each interacting with its first and second nearest neighbors. The long-range interaction between second nearest neighbors is assumed to be harmonic and attractive, while the first neighbor interactions are nonlinear and bistable. In the overdamped dynamics limit after a suitable rescaling this problem reduces to a discrete reaction-diffusion equation that corresponds to (1.1) with $d_1 < 0$ and $d_2 = 0$. In a related work, dynamics of periodic patterns in a variant of Frenkel-Kontorova model motivated by the dynamics of twin boundaries in certain superconductors is investigated in [24]; see also [25]. The model involves attractive harmonic interactions between second neighbors and nonconvex first-neighbor interactions that compete with a periodic substrate potential. In another related study [12] periodic structures with period given by a multiple of four are considered for a related elastically hinged molecule model with second-neighbor interactions, and domain-wall solutions involving the periodic patterns are constructed as kink solutions of a sine-Gordon equation obtained in the continuum approximation of the model.

Motivated by our earlier work [31], we focus much of our attention on the case where at least one of the interactions is repulsive (d_1 and/or d_2 are negative). This is certainly not a
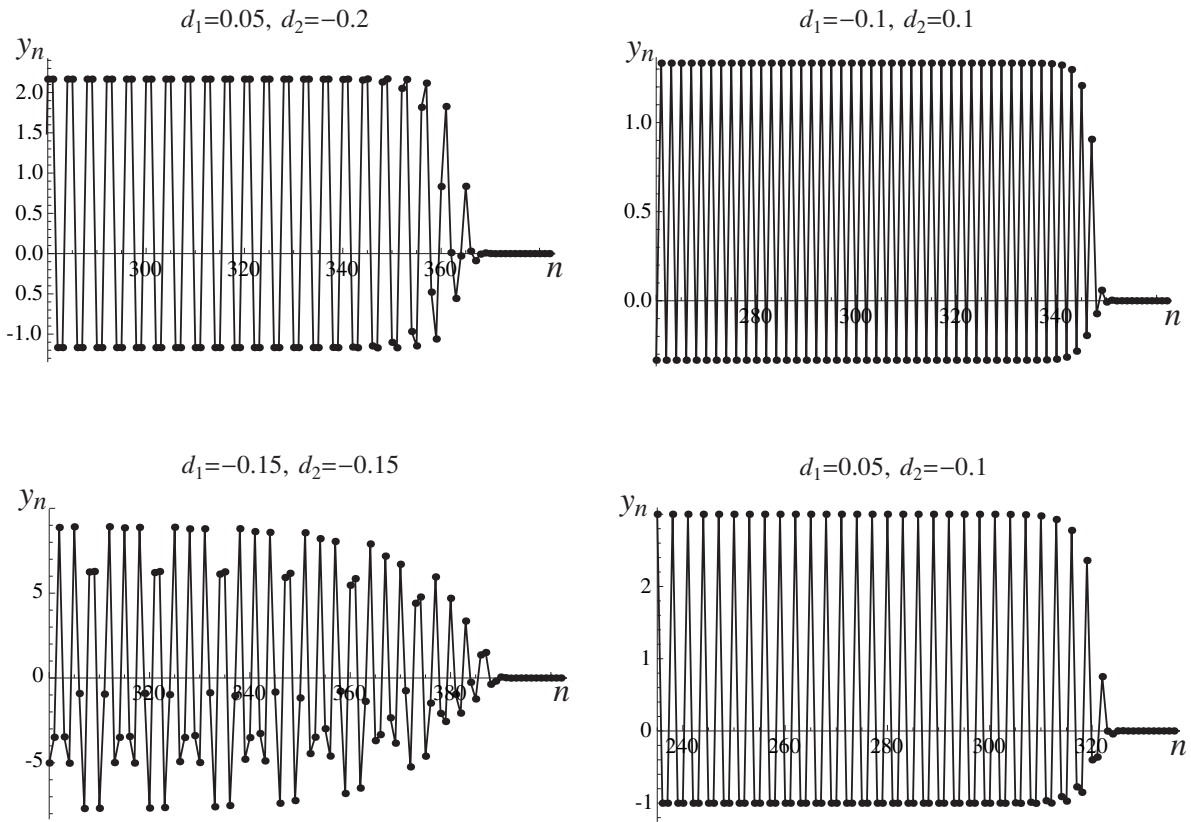
Figure 2. *Snapshots of solutions of* (1.1) *with* (1.2) *at* $a = 0.1$, $t = 200$ *and different values of* d_1 *and* d_2. *Only the enlarged view of the right front is shown in each panel. The initial conditions are shown in Fig. 1a.*

necessary condition for pattern formation: for example, one-dimensional 'checkerboard' equilibrium patterns with period $p = 2$ may exist even in the case $d_1 > 0$, $d_2 = 0$ [8], and we also discuss conditions for existence and propagation of such patterns when d_1 and d_2 are both positive. The possibility of negative elastic moduli for some long-range interactions is suggested by linearization of the Lennard-Jones potential [2]. Problems of this type can be thought of as antiferromagnetic Ising models with elastic wells, and ground states in such systems are of much interest in condensed matter physics [1, 20, 26]. We also note here that the use of second-neighbor interactions in addition to first-neighbor interactions provides an improved approximation to discrete convolution operators (with potentially infinite-range interactions) used to model either attactive or repulsive interactions, and the change in dynamics due to second-neighbor interactions is relatively unexplored. To ensure stability of the equilibrium states in the case when some moduli are negative, the coefficients must take values in a certain parameter region.

Using a bilinear bistable nonlinearity like the one considered here and the method suggested in [8] for the first-neighbor problem ($d_2 = 0$), traveling wave solutions connecting patterns of period $p = 2$ and the homogeneous equilibrium state are constructed in [31] for the case $d_1 < 0$. By rewriting the repulsive first-neighbor system with cubic nonlinearity as a

periodic media problem to employ the results in [10], the existence, multiplicity, and stability of connecting orbits between $p = 2$ periodic patterns is investigated in [6]. It is shown that these connecting orbits may correspond to both bistable and monostable dynamics. It is not difficult to see that results for connecting orbits between $p = 2$ patterns for $d_1 < 0$ and $d_2 = 0$ can be extended to $d_1 < 0$ and $d_2 > 0$. The results in [2] on infinite-range interactions with smooth bistable nonlinearities apply in the case considered here when $d_1 + 4d_2 > 0$. The paper [32] extends the ideas in [2] by employing reference solutions of differential-delay type to cases in which $d_1 < 0$, $d_2 \approx 0$ and $d_1 \approx 0$, $d_2 < 0$. Existence of traveling wave solutions in higher space dimensions with repulsive first-neighbor interactions when the direction of propagation is rational can be established using the results in [10], while the results in [19] may be employed to show existence when the the direction of propagation is irrational. Patterns occurring in discrete problems described by equations of Nagumo and Cahn-Hilliard type equations with both first and second-neighbor interactions are investigated in [7] on bounded two-dimensional domains. While the equations we consider here are in some sense analogous to semilinear backward parabolic equations, similar patterns are obtained in [11] using the analogue of quasilinear equations with bilinear nonlinearities.

We are interested in existence, global structure and multiplicity of traveling wave solutions of (1.1) that connect a stable p-periodic equilibrium solution to the stable zero equilibrium state and thus describe steady propagation of periodic patterns in the lattice. In this work we focus on the cases of $p = 2$, $p = 3$ and $p = 4$ but the method we use works equally well for larger p. We start by finding the periodic equilibria and identifying the range of parameters where these solutions and the homogeneous deformation states are stable. We then take advantage of the bilinear form of (1.2) and construct explicit traveling wave solutions using the Fourier transform technique. We conduct a detailed analysis of the solution in the $p = 2$ case and consider some examples in the $p = 3$ and $p = 4$ cases. In particular, we investigate the dependence of the detuning parameter a on the velocity c of the traveling wave and on the parameters d_1 and d_2.

In the case of competing interactions considered in this work we generally do not expect to have a comparison principle, a powerful tool that has been instrumental in the analysis of traveling wave solutions of reaction-diffusion type equations. The approach taken in [8] to show the existence and uniqueness (up to translation) of monotone traveling wave solutions in discrete media with bilinear, bistable nonlinearity (1.2) was based on showing that monotonicity in the tails of the waveform implies using the comparison principle a monotone waveform. This provides a way to verify that the waveform crosses the value a at only one point, which is consistent with the assumption used to construct the waveform. In our case we assume that each component of the traveling wave solution crosses the value of a at most once. In the absence of monotonicity results, we must verify (as in [13]) that our candidate solutions, formally obtained via Fourier transform under this assumption, actually satisfy the assumed inequalities. Since the Fourier integrals are computed numerically, such verification can only be done within the error of the approximation. This provides a computer-assisted proof of the existence of traveling waves we seek but makes it difficult to state explicit theorems.

One of the new features we find is the *finite* maximum propagation speed of the $p = 2$ patterns in the case when both first and second-neighbor interactions have the same sign. In contrast, traveling wave solutions of the discrete Nagumo equation [16] and some of the

other solutions we study here exist for all velocities c with the corresponding a that tends to zero as c tends to infinity. We identify some parameter regimes where the relation between the wave speed and the detuning parameter a is monotone, implying a unique propagation velocity for given a within certain bounds. Another interesting result is that multiple traveling waves representing one of the $p = 4$ patterns may propagate with the same speed (and slightly different detuning parameters) provided it is contained within a certain interval. Numerical simulations indicate stability of some of the obtained solutions and also suggest the existence of more complex dynamic solutions where not all components propagate with the same speed.

The remainder of the paper is organized as follows. In Sec. 2 we reformulate the problem in the vector form convenient for studying dynamics of the periodic patterns. In Sec. 3 we derive the necessary and sufficient conditions for stability of periodic and homogeneous equilibrium states. We find the periodic equilibria and the domains of their existence within the stability region in Sec. 4. Traveling wave solutions are constructed in Sec. 5. A detailed analysis of $p = 2$ case is presented in Sec. 6, with some technical details included in Appendix A. Examples and analysis of some solutions in $p = 3$ and $p = 4$ cases can be found in Sec. 7 and Sec. 8, respectively. Sec. 9 contains some concluding remarks.

2. Formulation. To construct traveling wave solutions connecting a stable p-periodic equilibrium state to the stable $y_n \equiv 0$ state, it is convenient to introduce for a given p a vector $\mathbf{u}_m \in \mathbb{R}^p$ with components

$$u_{m_j} = y_{pm+j-1}, \quad j = 1, \ldots, p$$

and rewrite (1.1) in the matrix form

$$\text{(2.1)} \qquad\qquad \dot{\mathbf{u}}_m = \mathbf{A}_{-1}\mathbf{u}_{m-1} + \mathbf{A}_0\mathbf{u}_m + \mathbf{A}_{+1}\mathbf{u}_{m+1} + \mathbf{h}(\mathbf{u}_m),$$

where $\mathbf{h}(\mathbf{u}_m) \in \mathbb{R}^p$ has components

$$\text{(2.2)} \qquad\qquad h_j(\mathbf{u}_m) = \theta(u_{m_j} - a), \quad j = 1, \ldots, p,$$

and the $p \times p$ matrices $\mathbf{A}_{-1}$, $\mathbf{A}_0$ and $\mathbf{A}_{+1}$ have the form
(2.3)
$$\mathbf{A}_{-1} = \begin{pmatrix} d_2 & d_1 \\ 0 & d_2 \end{pmatrix}, \quad \mathbf{A}_{+1} = \begin{pmatrix} d_2 & 0 \\ d_1 & d_2 \end{pmatrix}, \quad \mathbf{A}_0 = \begin{pmatrix} -(1 + 2d_1 + 2d_2) & d_1 \\ d_1 & -(1 + 2d_1 + 2d_2) \end{pmatrix}$$

at $p = 2$,

$$\text{(2.4)} \qquad\qquad \mathbf{A}_{-1} = \begin{pmatrix} 0 & d_2 & d_1 \\ 0 & 0 & d_2 \\ 0 & 0 & 0 \end{pmatrix}, \quad \mathbf{A}_{+1} = \begin{pmatrix} 0 & 0 & 0 \\ d_2 & 0 & 0 \\ d_1 & d_2 & 0 \end{pmatrix},$$

$$\text{(2.5)} \qquad \mathbf{A}_0 = \begin{pmatrix} -(1 + 2d_1 + 2d_2) & d_1 & d_2 \\ d_1 & -(1 + 2d_1 + 2d_2) & d_1 \\ d_2 & d_1 & -(1 + 2d_1 + 2d_2) \end{pmatrix}$$

at $p = 3$, and

$$(2.6) \qquad \mathbf{A}_{-1} = \begin{pmatrix} 0 & 0 & d_2 & d_1 \\ 0 & 0 & 0 & d_2 \\ 0 & 0 & 0 & 0 \\ 0 & 0 & 0 & 0 \end{pmatrix}, \qquad \mathbf{A}_{+1} = \begin{pmatrix} 0 & 0 & 0 & 0 \\ 0 & 0 & 0 & 0 \\ d_2 & 0 & 0 & 0 \\ d_1 & d_2 & 0 & 0 \end{pmatrix},$$

$$(2.7) \quad \mathbf{A}_0 = \begin{pmatrix} -(1 + 2d_1 + 2d_2) & d_1 & d_2 & 0 \\ d_1 & -(1 + 2d_1 + 2d_2) & d_1 & d_2 \\ d_2 & d_1 & -(1 + 2d_1 + 2d_2) & d_1 \\ 0 & d_2 & d_1 & -(1 + 2d_1 + 2d_2) \end{pmatrix}$$

at $p = 4$. We will study traveling wave solutions of (2.1) that connect a periodic equilibrium state $\mathbf{u}_-$ to $\mathbf{u}_+ = \mathbf{0}$.

3. Stability of the equilibrium states. To determine the physically relevant parameter space, we need to analyze stability of the equilibrium states $y_n(t) \equiv y_n^e$, where y_n^e is either a homogeneous equilibrium state ($y_n^e \equiv 0$ or, if $a < 1$, $y_n^e \equiv 1$) or a periodic equilibrium state with components $y_n^e \neq a$. Linearizing (1.1) about such a state by considering $y_n(t) = y_n^e + z_n e^{-\mu t}$ with small enough z_n such that $\theta(y_n(t) - a) = \theta(y_n^e - a)$, we obtain the eigenvalue problem

$$-\mu z_n = d_1(z_{n+1} - 2z_n + z_{n-1}) + d_2(z_{n+2} - 2z_n + z_{n-2}) - z_n.$$

Seeking solutions in the form $z_n = e^{ink}$ as in [29], we obtain

$$(3.1) \qquad \mu = 4(d_1 \sin^2(k/2) + d_2 \sin^2 k) + 1.$$

Stability requires that $\mu(k) > 0$ for all $k \in [0, \pi]$ (due to the reflectional symmetry and periodicity it suffices to consider wave numbers in only this interval). This holds if and only if

$$\min_{[0,\pi]} \mu(k) > 0,$$

which, in view of $\mu(0) = 1 > 0$, holds whenever $\mu(\pi) > 0$ and $\mu(k) > 0$ for all $k \in (0, \pi)$ such that $\mu'(k) = 0$ and $\mu''(k) > 0$. Now, the first condition, $\mu(\pi) > 0$, holds if and only if

$$(3.2) \qquad 1 + 4d_1 > 0.$$

It fails when $d_1 = -1/4$ and the corresponding instability eigenmode is $z_n = (-1)^n$. Consider now the second condition. Clearly, $\mu'(k) = 2 \sin k (d_1 + 4d_2 \cos k) = 0$ in $(0, \pi)$ whenever

$$(3.3) \qquad \cos k = -\frac{d_1}{4d_2},$$

which can only happen if

$$(3.4) \qquad -1 < -\frac{d_1}{4d_2} < 1.$$

Next, (3.3) implies that $\mu''(k) = -8d_2 \sin^2 k$, so that for $k \in (0, \pi)$ we have $\mu''(k) > 0$ (a minimum) only if $d_2 < 0$, which reduces (3.4) to

$$(3.5) \qquad\qquad 4d_2 < d_1 < -4d_2.$$

Thus, if (3.5) holds (at $d_2 < 0$), we must have $\mu(\arccos(-d_1/(4d_2))) > 0$, which yields

$$4d_2 + (d_1 + 4d_2)^2 < 0$$

or, in view of (3.5),

$$(3.6) \qquad\qquad d_2 > -\frac{1}{8}(1 + 2d_1 + \sqrt{1 + 4d_1}) \quad \text{for } 4d_2 < d_1 < -4d_2.$$

This condition fails when $z_n = e^{ink}$, $k = \arccos(-d_1/(4d_2))$, an incommensurate instability mode.

Together, the conditions (3.2) and (3.6) constitute the two necessary and sufficient conditions for stability of the homogeneous states. The stability domain in (d_1, d_2) parameter plane is shown in Fig. 3, and the parameters we consider in what follows must lie within this domain.
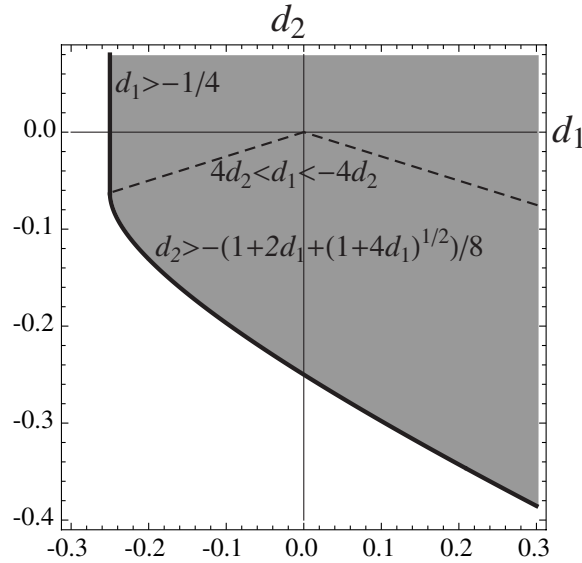

Figure 3. *Stability domain for the equilibrium states.*

4. Periodic Equilibrium Solutions. We now consider periodic equilibria of (2.1), which correspond to $\mathbf{u}_m \equiv \mathbf{u}$, where $\mathbf{u} \in \mathbb{R}^p$ is a constant vector. The problem then reduces to solving the linear system $\mathbf{A}\mathbf{u} = \mathbf{b}$, where $\mathbf{A} = -\mathbf{A}_{-1} - \mathbf{A}_0 - \mathbf{A}_{+1}$, and the vector $\mathbf{b} \in \mathbb{R}^p$ has components $b_j \in \{0, 1\}$ for $j = 1, \ldots, p$. Here $b_j = 0$ corresponds to the jth component of $\mathbf{u}$ satisfying the inequality $u_j < a$, so that $f(u_j) = u_j$, while $b_j = 1$ corresponds to $u_j > a$, so

that $f(u_j) = u_j - 1$. Thus, the components of $\mathbf{u} = \mathbf{A}^{-1}\mathbf{b}$, assuming that $\mathbf{A}$ is invertible, must satisfy

$$(4.1) \qquad\qquad u_j < a \quad \text{if } b_j = 0, \qquad u_j > a \quad \text{if } b_j = 1.$$

Recall that $a > 0$ and in what follows we assume $u_j \neq 0$. Together with (4.1), this implies

$$(4.2) \qquad a_{min} < a < a_{max}, \quad \text{where } a_{min} = \max_j\{0, u_j | b_j = 0\} \text{ and } a_{max} = \min_j\{u_j | b_j = 1\}.$$

Along with the conditions ensuring that $\mathbf{A}$ is invertible, these constraints determine the domains of existence of periodic equilibrium states in the parameter space (d_1, d_2, a). We remark that such a may satisfy $a > 1$, in which case a periodic equilibrium coexists with only one uniform equilibrium state, $y_n \equiv 0$. In what follows, we focus primarily on the *subset* of periodic equilibria that satisfy (4.2) with $a_{min} = 0$, that is,

$$(4.3) \qquad 0 < a < a_{max}, \quad \text{where } \max_j\{u_j | b_j = 0\} < 0 \text{ and } a_{max} = \min_j\{u_j | b_j = 1\}.$$

Such periodic equilibrium states exist in certain domains in the (d_1, d_2) plane for all a in $(0, a_{\max})$. In the examples considered below imposing conditions (4.3) results in at least one of the coefficients d_1 and d_2 being negative, the case that we mainly focus on in this work. However, periodic equilibria also exist when d_1 and d_2 are both positive, provided that the inequalities (4.2) hold along with the invertibility conditions.

A necessary condition for stability of an equilibrium is that all eigenvalues of $\mathbf{A}$ are positive (recall that $\mathbf{A}$ is negative of the sum of matrices in (1.1)) since it implies stability with respect to periodic perturbations that have the same period. In what follows we consider separately the cases $p = 2$, $p = 3$ and $p = 4$. As we will see, positive eigenvalues of $\mathbf{A}$ and therefore its invertibility are implied by (3.2) and (3.6), which, as we recall, constitute necessary and sufficient conditions for stability of both periodic and homogeneous equilibria.

4.1. 2-periodic equilibria. In the case $p = 2$ (2.3) yields $\mathbf{A} = -\mathbf{A}_{-1} - \mathbf{A}_0 - \mathbf{A}_{+1}$ given by

$$\mathbf{A} = \begin{pmatrix} 1 + 2d_1 & -2d_1 \\ -2d_1 & 1 + 2d_1 \end{pmatrix}.$$

Note that $\det\mathbf{A} = 1 + 4d_1 > 0$ by (3.2), so $\mathbf{A}$ is invertible, and we obtain

$$\mathbf{u} = \frac{1}{1 + 4d_1} \begin{pmatrix} (1 + 2d_1)b_1 + 2d_1 b_2 \\ 2d_1 b_1 + (1 + 2d_1)b_2 \end{pmatrix}.$$

There are only two nonhomogeneous periodic equilibria in this case. For $\mathbf{b} = (1, 0)$ we have

$$(4.4) \qquad\qquad \mathbf{u} = \frac{1}{1 + 4d_1} \begin{pmatrix} 1 + 2d_1 \\ 2d_1 \end{pmatrix},$$

and for $\mathbf{b} = (0, 1)$ the components of $\mathbf{u}$ are reversed. The conditions (4.3) then yield $d_1 < 0$ and $1 + 2d_1 > 0$, where the latter is automatically satisfied at negative d_1 due to (3.2), and

$$(4.5) \qquad\qquad 0 < a < \frac{1 + 2d_1}{1 + 4d_1},$$

where the upper bound is the positive component of (4.4). Observe also that the eigenvalues of $\mathbf{A}$, $\lambda_1 = 1$ and $\lambda_2 = 1 + 4d_1$, are always positive due to (3.2).

The domain of existence of stable nonhomogeneous $p = 2$ equilibrium states satisfying (4.3) is thus given by $d_1 < 0$, (3.2) and (3.6) and occupies the regions A-F in Fig. 4 with a in (4.5). We remark that stable nonhomogeneous $p = 2$ equilibria also exist in the domain defined by the inequalities $d_1 > 0$ and (3.6), provided that

$$(4.6) \qquad \frac{2d_1}{1 + 4d_1} < a < \frac{1 + 2d_1}{1 + 4d_1}.$$

A: $(1, 0, 1, 0), (1, 0)$

B: $(1, 1, 1, 0), (1, 0, 1, 0), (1, 0)$

C: $(1, 0, 1, 0), (1, 1, 1, 0),$
$(1, 0, 0), (1, 1, 0), (1, 0)$

D: $(1, 0, 1, 0), (1, 1, 0, 0),$
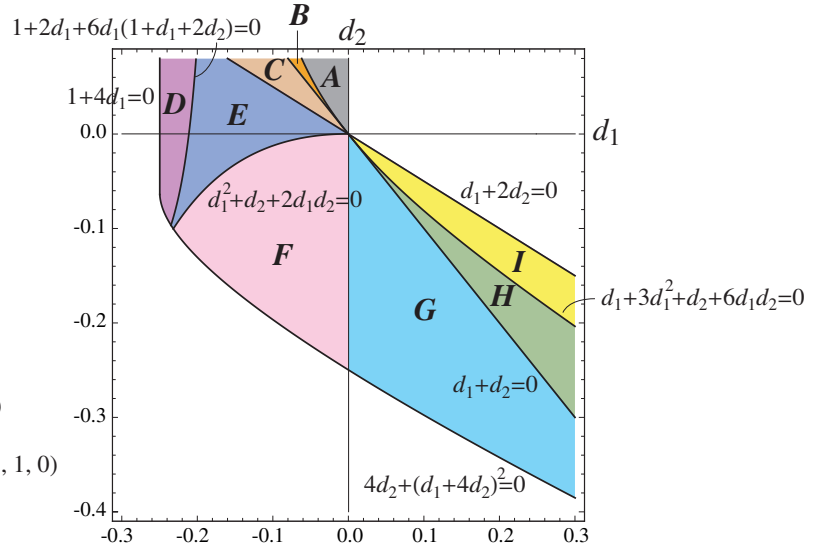$(1, 0, 0), (1, 1, 0), (1, 0)$

E: $(1, 0, 1, 0), (1, 1, 0, 0), (1, 1, 1, 0),$
$(1, 0, 0), (1, 1, 0), (1, 0)$

F: $(1, 0, 0, 0), (1, 1, 0, 0), (1, 0, 1, 0),$
$(1, 1, 1, 0), (1, 0, 0), (1, 1, 0), (1, 0)$

G: $(1, 1, 0, 0), (1, 1, 1, 0), (1, 0, 0), (1, 1, 0)$

H: $(1, 1, 0, 0), (1, 1, 1, 0)$

I: $(1, 1, 0, 0)$

Figure 4. *Domains of (co)existence of stable nonhomogeneous periodic equilibrium states satisfying (4.3). The legend on the left shows the values of $\mathbf{b}$ (up to a cyclic permutation) corresponding to the equilibria in each region.*

4.2. 3-periodic equilibria. At $p = 3$ we have $\mathbf{A}_{\pm 1}$ and $\mathbf{A}_0$ given by (2.4) and (2.5), respectively, so we obtain

$$\mathbf{A} = \begin{pmatrix} 1 + 2d_1 + 2d_2 & -d_1 - d_2 & -d_1 - d_2 \\ -d_1 - d_2 & 1 + 2d_1 + 2d_2 & -d_1 - d_2 \\ -d_1 - d_2 & -d_1 - d_2 & 1 + 2d_1 + 2d_2 \end{pmatrix}$$

with eigenvalues $\lambda_1 = 1$, $\lambda_2 = \lambda_3 = 1 + 3(d_1 + d_2)$. Note that $1 + 3(d_1 + d_2) > 0$ is implied by the stability condition (3.6), so $\mathbf{A}$ is invertible. Solving $\mathbf{A}\mathbf{u} = \mathbf{b}$ by Gaussian elimination, we obtain

$$\mathbf{u} = \frac{1}{1 + 3X} \begin{pmatrix} (1 + X)b_1 + Xb_2 + Xb_3 \\ Xb_1 + (1 + X)b_2 + Xb_3 \\ Xb_1 + Xb_2 + (1 + X)b_3 \end{pmatrix},$$

where $X = d_1 + d_2$. For $\mathbf{b} = (1, 0, 0)$, we obtain

$$\text{(4.7)} \qquad \mathbf{u} = \frac{1}{1 + 3(d_1 + d_2)} \begin{pmatrix} 1 + d_1 + d_2 \\ d_1 + d_2 \\ d_1 + d_2 \end{pmatrix},$$

with (4.3) and $1 + 3(d_1 + d_2) > 0$ established above requiring that $d_1 + d_2 < 0$ and

$$\text{(4.8)} \qquad 0 < a < \frac{1 + d_1 + d_2}{1 + 3d_1 + 3d_2}.$$

Thus the inequalities $d_1 + d_2 < 0$, (3.2) and (3.6) define the domain of existence of this equilibrium state, along with the equilibria corresponding to $\mathbf{b} = (0, 1, 0)$ and $\mathbf{b} = (0, 0, 1)$ obtained by the corresponding cyclic permutation of the components of $\mathbf{u}$, for a in (4.8). The domain corresponds to the regions C-G in Fig. 4.

Another nonhomogeneous periodic equilibrium state corresponds to $\mathbf{b} = (1, 1, 0)$ and is given by

$$\text{(4.9)} \qquad \mathbf{u} = \frac{1}{1 + 3(d_1 + d_2)} \begin{pmatrix} 1 + 2(d_1 + d_2) \\ 1 + 2(d_1 + d_2) \\ 2(d_1 + d_2) \end{pmatrix}.$$

In this case (4.3) and $1 + 3(d_1 + d_2) > 0$ again yield $d_1 + d_2 < 0$, and so the existence domain is again given by the regions C-G in Fig. 4 for this state and the ones obtained by cyclic permutation of the components, but now

$$\text{(4.10)} \qquad 0 < a < \frac{1 + 2d_1 + 2d_2}{1 + 3d_1 + 3d_2}.$$

4.3. 4-periodic equilibria. In the case $p = 4$ we have $\mathbf{A}_{\pm 1}$ and $\mathbf{A}_0$ given by (2.6) and (2.7), respectively, and therefore

$$\mathbf{A} = \begin{pmatrix} 1 + 2d_1 + 2d_2 & -d_1 & -2d_2 & -d_1 \\ -d_1 & 1 + 2d_1 + 2d_2 & -d_1 & -2d_2 \\ -2d_2 & -d_1 & 1 + 2d_1 + 2d_2 & -d_1 \\ -d_1 & -2d_2 & -d_1 & 1 + 2d_1 + 2d_2 \end{pmatrix}.$$

One can show that the eigenvalues are $\lambda_1 = 1$, $\lambda_2 = 1 + 4d_1$ and $\lambda_3 = \lambda_4 = 1 + 2d_1 + 4d_2$. Observe that (3.2) and (3.6) imply that all eigenvalues are positive, so $\mathbf{A}$ is invertible. Using Gaussian elimination and some algebra, we obtain

$$u_1 = (b_2 + b_4)d_1/(1 + 4d_1) + [b_1(1 + 4d_1 + Y) + b_3Y]/[(1 + 2d_1 + 4d_2)(1 + 4d_1)]$$
$$u_2 = (b_1 + b_3)d_1/(1 + 4d_1) + [b_2(1 + 4d_1 + Y) + b_4Y]/[(1 + 2d_1 + 4d_2)(1 + 4d_1)]$$
$$u_3 = (b_2 + b_4)d_1/(1 + 4d_1) + [b_3(1 + 4d_1 + Y) + b_1Y]/[(1 + 2d_1 + 4d_2)(1 + 4d_1)]$$
$$u_4 = (b_1 + b_3)d_1/(1 + 4d_1) + [b_4(1 + 4d_1 + Y) + b_2Y]/[(1 + 2d_1 + 4d_2)(1 + 4d_1)]$$

where

$$Y = 2(d_1^2 + 2d_1d_2 + d_2).$$

When $d_1 = 2d_2$, we have $Y = d_1(1 + 4d_1)$, and the expressions simplify to $u_j = (d_1\bar{b} + b_j)/(1 + 4d_1)$ for $j = 1, \ldots, 4$, where $\bar{b} = b_1 + b_2 + b_3 + b_4$.

We now obtain the existence conditions for nonhomogeneous periodic equilibria satisfying (4.3). As before, since a cyclic permutation of the components of $\mathbf{b}$ yields a solution with the same permutation of components of $\mathbf{u}$, it suffices to consider only $\mathbf{b} = (1, 0, 0, 0)$, $(1, 1, 0, 0)$, $(1, 0, 1, 0)$ and $(1, 1, 1, 0)$. For $\mathbf{b} = (1, 0, 0, 0)$ we obtain

(4.11)
$$u_1 = \frac{1 + 4d_1 + Y}{(1 + 2d_1 + 4d_2)(1 + 4d_1)}, \quad u_2 = u_4 = \frac{d_1}{1 + 4d_1}, \quad u_3 = \frac{Y}{(1 + 2d_1 + 4d_2)(1 + 4d_1)}$$

Observe that (3.2) and (3.6) ensure that the denominator is positive for each component and that $1 + 4d_1 + Y > 0$, so that the first component is positive. In addition, (4.3) requires that the remaining components are negative, which means $d_1 < 0$ and $Y < 0$, and that

(4.12)
$$0 < a < \frac{1 + 4d_1 + 2(d_1^2 + 2d_1 d_2 + d_2)}{(1 + 2d_1 + 4d_2)(1 + 4d_1)}.$$

Together with (3.2) and (3.6) these inequalities define the existence domain of this equilibrium state, which occupies the region F in Fig. 4, with a in (4.12).

For $\mathbf{b} = (1, 1, 0, 0)$, we obtain

(4.13)
$$u_1 = u_2 = \frac{1 + d_1 + 2d_2}{1 + 2d_1 + 4d_2}, \quad u_3 = u_4 = \frac{d_1 + 2d_2}{1 + 2d_1 + 4d_2}.$$

One can see that the existence domain in this case is given by $d_1 + 2d_2 < 0$, (3.2) and (3.6) since these also imply $1 + d_1 + 2d_2 > 0$, and occupies the regions D-I in Fig. 4, with

(4.14)
$$0 < a < \frac{1 + d_1 + 2d_2}{1 + 2d_1 + 4d_2}.$$

For $\mathbf{b} = (1, 0, 1, 0)$ the equilibrium is simply the 4-periodic extension of the 2-periodic equilibrium considered above, with

(4.15)
$$u_1 = u_3 = \frac{1 + 2d_1}{1 + 4d_1}, \quad u_2 = u_4 = \frac{2d_1}{1 + 4d_1}$$

and the same existence domain (regions A-F in Fig. 4), with a in (4.5).

Finally, we consider $\mathbf{b} = (1, 1, 1, 0)$, which yields

$$u_1 = u_3 = \frac{1 + 3d_1}{1 + 4d_1}, \quad u_2 = \frac{1 + 2d_2 + 6d_1(1 + d_1 + 2d_2)}{(1 + 4d_1)(1 + 2d_1 + 4d_2)}, \quad u_4 = \frac{2(d_1 + 3d_1^2 + d_2 + 6d_1 d_2)}{(1 + 4d_1)(1 + 2d_1 + 4d_2)}.$$

Note that (3.2) ensures that the first and third components are positive, and (3.2) and (3.6) imply that the denominators in the second and fourth components are positive. Thus $1 + 2d_2 + 6d_1(1 + d_1 + 2d_2) > 0$ and $d_1 + 3d_1^2 + d_2 + 6d_1 d_2 < 0$ ensure that the second component is positive and the fourth is negative. Together with (3.2) and (3.6), these inequalities define the existence domain of this equilibrium state, which occupies the regions B,C, E-H. In this case $0 < a < \min\{u_1, u_2\}$.

5. Traveling wave solutions. We now consider traveling waves of (2.1) connecting a non-homogeneous periodic equilibrium state $\mathbf{u}^- \in \mathbb{R}^p$ to $\mathbf{u}^+ = \mathbf{0}$. The solutions have the form

$$(5.1) \qquad\qquad \mathbf{u}_m(t) = \boldsymbol{\varphi}(\xi), \quad \xi = m - ct,$$

where $c \neq 0$ is the velocity of the wave, and satisfy

$$(5.2) \qquad\qquad \boldsymbol{\varphi}(\xi) \to \mathbf{u}^- \quad \text{as } \xi \to -\infty, \quad \boldsymbol{\varphi}(\xi) \to \mathbf{0} \quad \text{as } \xi \to +\infty.$$

Substituting (5.1) in (2.1), we obtain

$$-c\boldsymbol{\varphi}'(\xi) = \sum_{k=-1}^{1} \mathbf{A}_k \boldsymbol{\varphi}(\xi + k) + \mathbf{h}(\boldsymbol{\varphi}(\xi)).$$

Taking the (generalized) Fourier transform

$$\hat{\boldsymbol{\varphi}}(s) = \lim_{\varepsilon \to 0+} \int_{-\infty}^{+\infty} e^{-i(s+i\varepsilon)\xi} \boldsymbol{\varphi}(\xi) d\xi,$$

we obtain

$$(5.3) \qquad\qquad \mathbf{A}(s)\hat{\boldsymbol{\varphi}}(s) = \hat{\mathbf{h}}(s), \quad \mathbf{A}(s) \equiv -ics\mathbf{I} - \sum_{k=-1}^{1} e^{iks} \mathbf{A}_k$$

Next, observe that by (2.2) and (5.2), there are two possibilities for each component of $\mathbf{h}$:

$$h_j(\boldsymbol{\varphi}(\xi)) = \theta(\xi_j - \xi) \quad \text{or} \quad h_j(\boldsymbol{\varphi}(\xi)) = 0.$$

The first case, which by our assumptions must hold for at least one value of j, corresponds to a solution component that satisfies $\varphi_j(\xi_j) = a$, $\varphi_j(\xi) \gtrless a$, $\xi \lessgtr \xi_j$, while in the second case $\varphi_j(\xi) < a$ for all ξ. Here we assume that a solution component that crosses the value a does so at only one point ξ_j, which yields

$$(5.4) \qquad\qquad \hat{h}_j(s) = -\frac{e^{-is\xi_j}}{i(s + i0)},$$

where $s + i0$ denotes the limit of $s + i\varepsilon$ as $\varepsilon \to 0+$. Observe also that by our assumptions the number $l < p$ of such solution components equals the number of nonzero components of the vector $\mathbf{b}^-$ corresponding to the nonhomogeneous periodic equilibrium state $\mathbf{u}^-$; without loss of generality, we assume that $b_j^- = 1$ at $j = i_1, i_2, \ldots, i_l$. The other components of $\hat{\mathbf{h}}(s)$ are zero. From (5.3), the inverse Fourier transform gives us

$$(5.5) \qquad\qquad \boldsymbol{\varphi}(\xi) = \frac{1}{2\pi} \int_\Gamma e^{is\xi} \mathbf{A}^{-1}(s) \hat{\mathbf{h}}(s) ds,$$

where Γ is the contour in the complex plane goes to along the real axis everywhere except near the origin where it goes in a small semicircle above it to resolve the singularity as prescribed by (5.4). By above,

$$(5.6) \qquad \varphi_j(\xi_j) - a = 0, \quad j = i_1, i_2, \ldots, i_l.$$

Due to translational invariance, we can always set $\xi_{i_1} = 0$. For given c, (5.6) is a system of l algebraic equations for l unknowns a, ξ_j, $j = i_2, \ldots, i_l$. Thus the existence of solutions of (5.6) gives the candidates for traveling wave solutions. To get the existence of traveling wave solutions, we must verify that

$$(5.7) \qquad \begin{cases} \varphi_j(\xi) < a & \text{for all } \xi, \quad j \in \{i|b_i = 0\}, \\ \varphi_j(\xi) \gtrless a & \text{for } \xi \lessgtr \xi_j, \quad j \in \{i|b_i = 1\}, \end{cases}$$

and that $a_{min} < a < a_{max}$ with the bounds defined in (4.2).

In what follows, we describe in detail the case $p = 4$; the cases $p = 3$ and $p = 2$ are treated similarly.

The specific form (2.6) and (2.7) of the matrices $\mathbf{A}_k$ in (2.1) at $p = 4$ yields

$$\mathbf{A}(s) = \begin{pmatrix} D(s) & -d_1 & -d_2(1 + e^{-is}) & -d_1 e^{-is} \\ -d_1 & D(s) & -d_1 & -d_2(1 + e^{-is}) \\ -d_2(1 + e^{is}) & -d_1 & D(s) & -d_1 \\ -d_1 e^{is} & -d_2(1 + e^{is}) & -d_1 & D(s) \end{pmatrix},$$

where $D(s) = 1 + 2d_1 + 2d_2 - ics$. Note that $\mathbf{A}(s)$ has the block form

$$\mathbf{A}(s) = \begin{pmatrix} \mathbf{B}(s) & \mathbf{C}(s) \\ \mathbf{C}^*(s) & \mathbf{B}(s) \end{pmatrix}, \quad \mathbf{B}(s) = \begin{pmatrix} D(s) & -d_1 \\ -d_1 & D(s) \end{pmatrix}, \quad \mathbf{C}(s) = -\begin{pmatrix} d_2(1 + e^{-is}) & d_1 e^{-is} \\ d_1 & d_2(1 + e^{-is}) \end{pmatrix},$$

We can now solve (5.3) using block Gaussian Elimination or block Cholesky to obtain

$$\begin{pmatrix} \hat{\varphi}_1(s) \\ \hat{\varphi}_2(s) \end{pmatrix} = \mathbf{B}^{-1}[\mathbf{I} + \mathbf{C}\mathbf{W}^{-1}\mathbf{C}^*\mathbf{B}^{-1}] \begin{pmatrix} \hat{h}_1(s) \\ \hat{h}_2(s) \end{pmatrix} - \mathbf{B}^{-1}\mathbf{C}\mathbf{W}^{-1} \begin{pmatrix} \hat{h}_3(s) \\ \hat{h}_4(s) \end{pmatrix},$$

$$\begin{pmatrix} \hat{\varphi}_3(s) \\ \hat{\varphi}_4(s) \end{pmatrix} = -\mathbf{W}^{-1}\mathbf{C}^*\mathbf{B}^{-1} \begin{pmatrix} \hat{h}_1(s) \\ \hat{h}_2(s) \end{pmatrix} + \mathbf{W}^{-1} \begin{pmatrix} \hat{h}_3(s) \\ \hat{h}_4(s) \end{pmatrix},$$

where $\mathbf{W} = \mathbf{B} - \mathbf{C}^*\mathbf{B}^{-1}\mathbf{C}$.

Taking inverse Fourier transform, we obtain

$$(5.8) \quad \begin{pmatrix} \varphi_1(\xi) \\ \varphi_2(\xi) \end{pmatrix} = \frac{1}{2\pi} \int_{\Gamma} e^{is\xi} \left[\mathbf{B}^{-1}[\mathbf{I} + \mathbf{C}\mathbf{W}^{-1}\mathbf{C}^*\mathbf{B}^{-1}] \begin{pmatrix} \hat{h}_1(s) \\ \hat{h}_2(s) \end{pmatrix} - \mathbf{B}^{-1}\mathbf{C}\mathbf{W}^{-1} \begin{pmatrix} \hat{h}_3(s) \\ \hat{h}_4(s) \end{pmatrix} \right] ds,$$

and

$$(5.9) \qquad \begin{pmatrix} \varphi_3(\xi) \\ \varphi_4(\xi) \end{pmatrix} = \frac{1}{2\pi} \int_{\Gamma} e^{is\xi} \left[-\mathbf{W}^{-1}\mathbf{C}^*\mathbf{B}^{-1} \begin{pmatrix} \hat{h}_1(s) \\ \hat{h}_2(s) \end{pmatrix} + \mathbf{W}^{-1} \begin{pmatrix} \hat{h}_3(s) \\ \hat{h}_4(s) \end{pmatrix} \right] ds.$$

For given velocity c, we can then determine the values of a and the unknown ξ_j from (5.6). As an example, consider the case $\mathbf{b}^- = (1,1,0,0)$ when the first and second components of $\hat{\mathbf{h}}$ are the only nonzero components. We can then set $\xi_1 = 0$ and treat ξ_2 as an unknown. To determine ξ_2 we note that $\varphi_1(0) = \varphi_2(\xi_2) = a$. Using the formulas (5.8), (5.9) for the solution, we define the function $g(\xi_2) \equiv \varphi_1(0) - \varphi_2(\xi_2)$ and seek ξ_2 such that $g(\xi_2) = 0$. These (possibly multiple) values of ξ_2 are then used to find the corresponding a from $\varphi_j(0) = a$. Similarly if the first, second, and third components of $\hat{\mathbf{h}}$ are the only nonzero components, we set $\xi_1 = 0$ and define

$$g_1(\xi_2, \xi_3) \equiv \varphi_1(0) - \varphi_2(\xi_2), \quad g_2(\xi_2, \xi_3) \equiv \varphi_1(0) - \varphi_3(\xi_3)$$

and seek ξ_2, ξ_3 such that g_1 and g_2 are zero. In some sense these are the bifurcation equations for the problem. Recall that we also need to check that for such ξ_2, ξ_3 the corresponding solution components only cross a at these points, as assumed.

Similarly, one can solve (5.3) when $p = 3$, with

$$\mathbf{A}(s) = \begin{pmatrix} D(s) & -d_1 - d_2 e^{-is} & -d_2 - d_1 e^{-is} \\ -d_1 - d_2 e^{is} & D(s) & -d_1 - d_2 e^{-is} \\ -d_2 - d_1 e^{is} & -d_1 - d_2 e^{is} & D(s) \end{pmatrix},$$

and when $p = 2$, with

$$\mathbf{A}(s) = \begin{pmatrix} 1 + 2d_1 + 4d_2 \sin^2(s/2) - ics & -d_1(1 + e^{-is}) \\ -d_1(1 + e^{is}) & 1 + 2d_1 + 4d_2 \sin^2(s/2) - ics \end{pmatrix},$$

and then invert the Fourier transform.

We now illustrate the obtained solution obtained via several examples. For simplicity, we limit our discussion to the case $c > 0$ unless stated otherwise.

6. The case $p = 2$. We start by considering traveling wave solutions that connect a 2-periodic equilibrium with $\mathbf{b}^- = (1,0)$ to $\mathbf{0}$. Recall that in this case $\mathbf{u}^-$ is given by (4.4) and that this solution exists and is stable when (3.6) holds and either $-1/4 < d_1 < 0$, with a bounded by (4.5), or $d_1 > 0$, with a satisfying (4.6).

We first consider the case when $-1/4 < d_1 < 0$, (3.6) and (4.5) are satisfied. In this case we have $\hat{h}_1 = -1/(i(s + i0))$ (setting $\xi_1 = 0$), $\hat{h}_2 = 0$, and the traveling wave solution is given by

$$(6.1) \qquad \begin{pmatrix} \varphi_1(\xi) \\ \varphi_2(\xi) \end{pmatrix} = -\frac{1}{2\pi i} \int_\Gamma \frac{e^{is\xi}}{sL(s,c)} \begin{pmatrix} 1 + 2d_1 + 4d_2 \sin^2(s/2) - ics \\ d_1(1 + e^{is}) \end{pmatrix} ds,$$

where

$$(6.2) \qquad L(s,c) = (1 + 2d_1 + 4d_2 \sin^2(s/2) - ics)^2 - 4d_1^2 \cos^2(s/2).$$

The requirement that $\varphi_1(0) = a$ then yields the following relation between a and c:

$$(6.3) \qquad a = \frac{1}{2\pi i} \int_\Gamma \frac{ics - 1 - 2d_1 - 4d_2 \sin^2(s/2)}{sL(s,c)} ds.$$

Recall that a must satisfy (4.5). Since c is related to a through (6.3), the bounds on a may impose some bounds on c. In addition, we must verify that the formal solutions satisfy the inequalities assumed to obtain them:

$$(6.4) \qquad\qquad \varphi_1(\xi) \gtrless a \quad \text{for } \xi \lessgtr 0, \qquad \varphi_2(\xi) < a.$$

In the case $d_2 = 0$ the solution (6.1) was studied in [31]. As in that work, we can compute (6.1), (6.3) in terms of the roots of $L(s, c) = 0$ that are contained inside the sets

$$(6.5) \qquad\qquad M^{\pm}(c) = \{s|\ L(s, c) = 0, \ \text{Im}\, s \gtrless 0\};$$

the resulting expressions are given by (A.1) and (A.2) in Appendix A, where the structure of the roots is also analyzed. Note that the sets (6.5) contain infinitely many roots and since the sums in (A.1) converge slowly near $\xi = 0$ as more roots are included, particularly at smaller c, it is more efficient to evaluate (6.1), (6.3) numerically in Mathematica using Levin's method for oscillatory integrals.

The resulting relation between a and c at $d_1 = -0.2$ and different values of d_2 is shown in Fig. 5a. Here and in what follows, $a(c)$ curves are shown only for solutions that satisfy the assumed inequalities, i.e. correspond to existing traveling waves. One can see that a
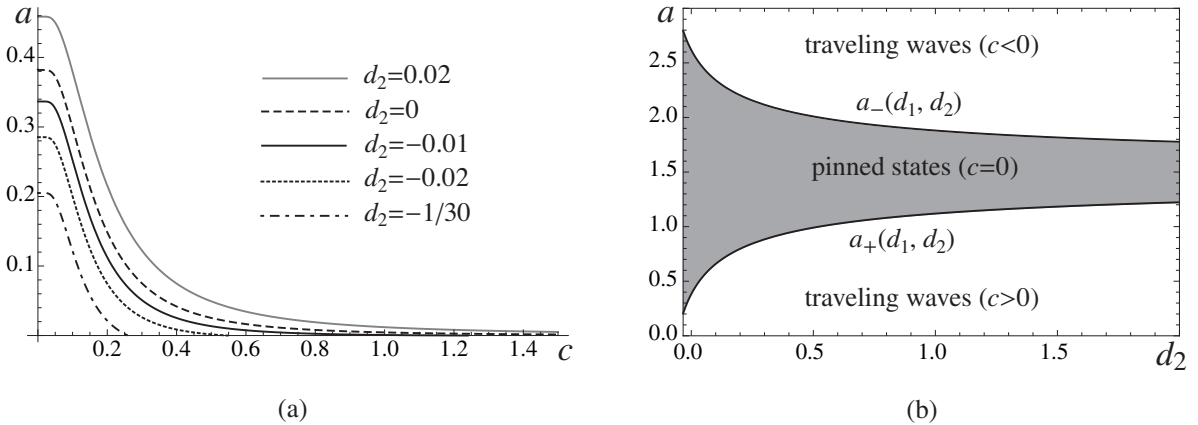
Figure 5. *(a) The relation $a(c)$ at $d_1 = -0.2$ and different values of d_2. (b) The regions of existence of traveling waves and pinned equilibrium states at $d_1 = -0.2$ for $d_2 \geq -1/30$.*

monotonically decreases as c grows and as $c \to 0+$, it approaches a constant value $a(0+)$, a depinning threshold, an explicit expression (6.8) for which is derived below. Traveling wave solutions exist for $0 < a < a(0+)$, and $a(0+)$ increases with d_2. In particular, at fixed a, the speed of the wave decreases with d_2 and for d_2 below a certain value that depends on a, there are only pinned stationary solutions with $c = 0$. Observe that at $d_2 \geq 0$, the curves look similar to the ones for heteroclinic ($p = 1$) traveling wave solutions of discrete Nagumo equation with $d_1 > 0$ and $d_2 = 0$ [16]. In particular, they tend to zero as $c \to \infty$. However, at $d_2 < 0$ a new feature emerges: a becomes zero at *finite* velocity c_{max}, which means that $p = 2$ traveling waves can only exist for $0 < c < c_{max}$. The value of c_{max} approaches infinity as $d_2 \to 0-$.

Some typical solution snapshots $y_n(t)$ obtained from the (shifted) traveling wave solution $\mathbf{u}_m(t) = (y_{2m}(t), y_{2m+1}(t)) = (\varphi_1(m - ct - 100), \varphi_2(m - ct - 100))$ are shown in Fig. 6 (solid lines) along with the results of numerical simulations (circles) of (2.1), (2.3) at the corresponding values of a with initial conditions given by the traveling waves. The excellent agreement between the numerical and analytical results (the difference between the two is on the order of 10^{-7} in the left panel and 10^{-8} in the right, while the difference between velocities in the numerical and analytical solutions is on the order of 10^{-9} in both cases) suggests stability of the traveling wave solution. This is confirmed by numerical simulations with more generic tanh-like initial data that also yield steady propagation with essentially the same velocity (difference on the order of 10^{-9}). Similar results were obtained for other values of c, d_1 and d_2.
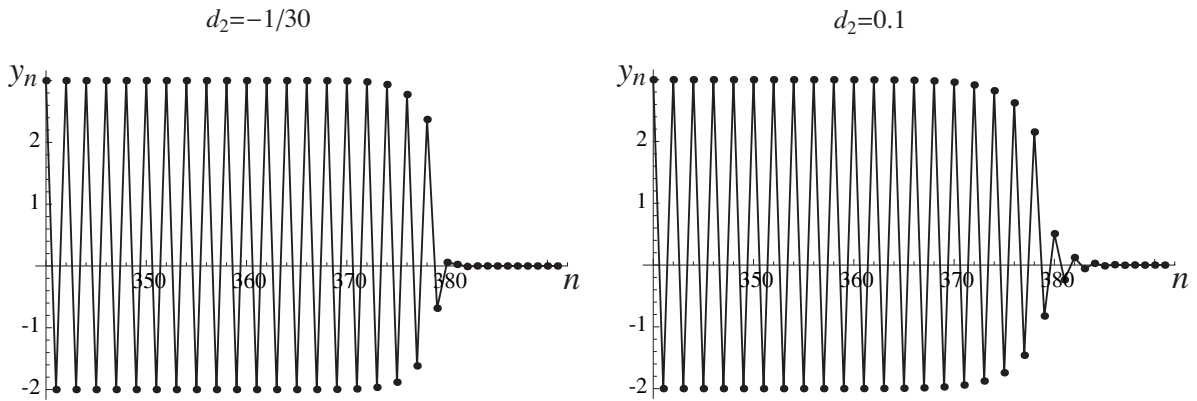
Figure 6. *Snapshots of numerical solution of* (2.1), (2.3) *(circles) and traveling wave solution (lines) at* $t = 600$ *corresponding to* $c = 0.15$, $d_1 = -0.2$ *and different values of* d_2. *Here* $a \approx 0.058$ *at* $d_2 = -1/30$ *and* $a \approx 0.508$ *at* $d_2 = 0.1$. *The numerical simulations were run with these values of* a *and the initial condition given by* $\mathbf{u}_m(0) = (y_{2m}(0), y_{2m+1}(0)) = (\varphi_1(m - 100), \varphi_2(m - 100))$.

In general, analyzing the roots in (6.5) one can show that larger d_2 yields wider boundary layers around the front (as can be seen by comparing left and right panels in Fig. 6) due to the smaller absolute values of the imaginary parts of the roots closest to the origin. As discussed in Appendix A, such roots are purely imaginary at $d_2 \geq 0$. Thus we expect $\varphi_1(\xi)$ and $\varphi_2(\xi)$ to be monotone, and the assumed inequalities (6.4) to always hold in view of the conditions at infinity and the constraints (4.5) on a. But at $d_2 < 0$ the roots in $\mathrm{Im}(s) > 0$ become complex at sufficiently large c, which leads to non-monotonicity of $\varphi_1(\xi)$ at $\xi > 0$ and of $\varphi_2(\xi)$ at $\xi > -1/2$ if the ratio of real and imaginary parts of the root closest to the origin in the first quadrant $(\mathrm{Im}(s) > 0, \mathrm{Re}(s) > 0)$ is large enough. When $d_2 < 0$ and $|d_2|$ is sufficiently large, this non-monotonicity of the (formal) solution results in violation of at least one of the assumed inequalities $\varphi_1(\xi) < a$ at $\xi > 0$ and $\varphi_2(\xi) < a$ for all ξ, thus rendering the solution inadmissible. An example of such solution failure is shown in Fig. 7, where $\varphi_2(\xi) < a$ is clearly violated at $d_1 = -0.2$, $d_2 = -0.05$ and $c = 0.1$.

In the limit $c \to 0+$, the traveling waves approach the stationary states that are pinned by the lattice $(c = 0)$. These are equilibrium solutions of (2.1), (2.3) that up to a shift in the

(a)   (b)
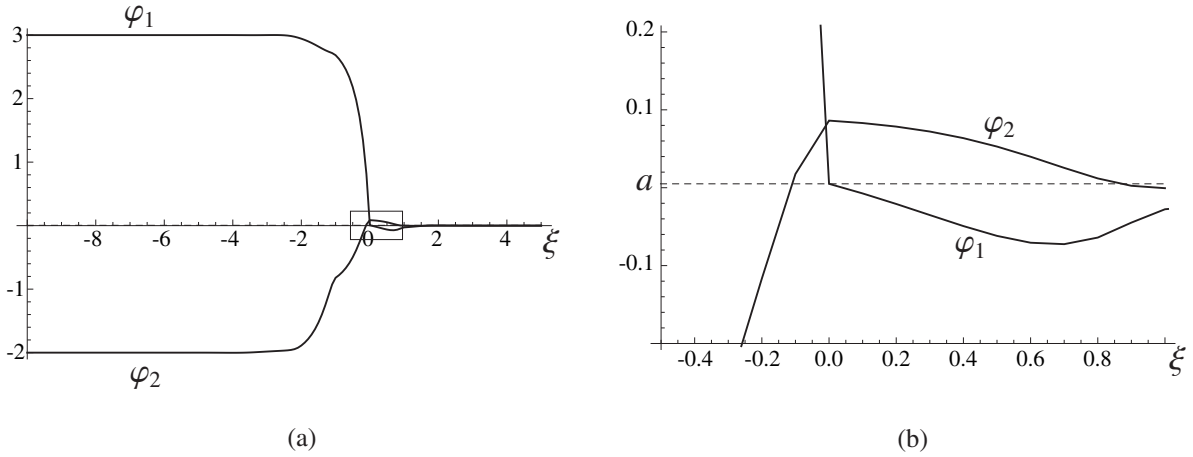
Figure 7. *(a) A formal solution* (6.1) *at* $d_1 = -0.2$, $d_2 = -0.05$ *and* $c = 0.1$, *which violates the assumed inequality* $\varphi_2(\xi) < a$; *(b) enlarged view inside the rectangle in (a). The dashed line marks* $a \approx 0.005$.

front location, satisfy the inequalities

$$(6.6) \qquad y_{2m} > a \quad \text{for } m \leq -1, \qquad y_{2m} < a \quad \text{for } m \geq 0, \qquad y_{2m+1} < a \quad \text{for all } m$$

for some a such that (4.5) holds. These solutions thus satisfy the difference equation

$$\mathbf{A}_{-1}\mathbf{u}_{m-1} + \mathbf{A}_0\mathbf{u}_m + \mathbf{A}_{+1}\mathbf{u}_{m+1} = -\begin{pmatrix} \theta(-m - 1/2) \\ 0 \end{pmatrix}$$

with $\mathbf{A}_k$ given by (2.3). Using discrete Fourier transform, we obtain $\mathbf{u}_m = (y_{2m}, y_{2m+1})$, with

$$(6.7) \qquad y_{2m} = \begin{cases} \dfrac{1 + 2d_1}{1 + 4d_1} + \displaystyle\sum_{s \in M_0^-} \dfrac{1 + 2d_1 + 4d_2 \sin^2(s/2)}{2\sin(s/2)L_0'(s)} e^{is(m+1/2)}, & m \leq -1 \\[3mm] -\displaystyle\sum_{s \in M_0^+} \dfrac{1 + 2d_1 + 4d_2 \sin^2(s/2)}{2\sin(s/2)L_0'(s)} e^{is(m+1/2)}, & m \geq 0, \end{cases}$$

$$y_{2m+1} = \begin{cases} \dfrac{2d_1}{1 + 4d_1} + d_1 \displaystyle\sum_{s \in M_0^-} \dfrac{\cos(s/2)}{\sin(s/2)L_0'(s)} e^{is(m+1)}, & m \leq -1 \\[3mm] -d_1 \displaystyle\sum_{s \in M_0^+} \dfrac{\cos(s/2)}{\sin(s/2)L_0'(s)} e^{is(m+1)}, & m \geq 0, \end{cases}$$

where $L_0(s) \equiv L(s,0)$ and the roots in $M_0^\pm = \{s|\, L_0(s) = 0,\ |\mathrm{Re}(s)| \leq \pi,\ \mathrm{Im}(s) \gtrless 0\}$ are given by (A.3), (A.4). The stationary solutions (6.7) exist for a satisfying (4.5) provided that a is such that the inequalities (6.6) hold. Similar to periodic and homogeneous equilibria, these solutions, when exist, are stable equilibrium states of (2.1) under the assumed stability conditions (3.2) and (3.6). At

$$d_2 \geq \frac{1}{8}\left(\sqrt{1 + 4d_1} - 1 - 2d_1\right)$$

the even and odd components of the stationary solution (6.7) are monotone sequences because the roots (A.3) are purely imaginary. Although the roots become complex for d_2 below the above threshold and are given by (A.4), the components remain monotone in a sufficiently large neighborhood around the front when $|d_2|$ is small enough. The monotonicity then implies that (6.6) are satisfied provided that $y_{-2} > a$ and $y_0 < a$, which means that stable stationary solutions exist whenever a is within the trapping region

$$a_+ < a < a_-,$$

where the lower limit,

(6.8)
$$a_+ = a(0+) = -\sum_{s \in M_0^+} \frac{1 + 2d_1 + 4d_2 \sin^2(s/2)}{2\sin(s/2)L_0'(s)} e^{is/2},$$

is a *depinning threshold* below which there exist traveling wave solutions with $c > 0$, and

$$a_- = a(0-) = \frac{1 + 2d_1}{1 + 4d_1} + \sum_{s \in M_0^-} \frac{1 + 2d_1 + 4d_2 \sin^2(s/2)}{2\sin(s/2)L_0'(s)} e^{-is/2}$$

is another depinning threshold above which the front starts moving to the left ($c < 0$). At the depinning values the equilibria become saddle points at which the traveling wave solutions bifurcate. The traveling waves with $c > 0$ thus exist for $0 < a < a_+(d_1, d_2)$, while the waves with $c < 0$ exist for $a_-(d_1, d_2) < a < (1 + 2d_1)/(1 + 4d_1)$, as illustrated in Fig. 5b.

For a more complete analysis of the $p = 2$ case, we now consider the case $d_1 > 0$. In this case the inequalities (4.3) no longer hold, and we impose the general inequalities (4.2) instead. For given $d_1 > 0$ and any d_2 satisfying (3.6) a stable periodic equilibrium state with $\mathbf{b}^- = (1, 0)$ then exists provided that a is bounded by (4.6). The traveling wave solutions, when exist, are still given by (6.1), (6.3) and must satisfy the inequalities (6.4) and (4.6).

We start with the case $d_1 > 0$, $d_2 \geq 0$. In this case by comparison principle together with a saddle structure in the linearization at the endpoints, both components of the traveling wave solution with positive wave speed, when it exists, must be monotone decreasing from the corresponding positive value to zero. The function $a(c)$ formally obtained from (6.3) is also monotone decreasing from the depinning value $a(0+) = a_+(d_1, d_2)$ given by (6.8) to zero. Thus if $a_+(d_1, d_2)$ satisfies (4.6), a traveling wave solution exist for $0 < c < c_{max}$, where c_{max} satisfies

$$a(c_{max}) = \frac{2d_1}{1 + 4d_1}.$$

So similar to the case when d_1 and d_2 are both negative, such waves can only propagate with velocities below a finite maximal value that depends on d_1 and d_2. It thus remains to find the parameter domain where $a_+(d_1, d_2)$ satisfies (4.6). One can show that for each $d_1 > 0$, $a_+(d_1, d_2)$ monotonely increases from the positive value $a_+(d_1, 0) = (1 + 2d_1 - \sqrt{1 + 4d_1})/(2 + 8d_1)$ to the limit $a_+^\infty(d_1) = (1 + 2d_1)/(2 + 8d_1)$ as $d_2 \geq 0$ tends to infinity, so a_+ is always below the upper bound in (4.6). Hence it is the inequality

$$a_+(d_1, d_2) > \frac{2d_1}{1 + 4d_1}$$

that determines the domain of existence of the traveling waves. This implies that for given d_1 within the range $0 < d_1 < 0.5$, traveling waves exist for $d_2 > d_2^*(d_1) \geq 0$, in the shaded region shown in Fig. 8a, so attractive second-neighbor interactions must be sufficiently strong. The curve $d_2^*(d_1)$ tends to infinity as $d_1 \to 0.5$ from below, and for $d_1 \geq 0.5$ there are no traveling wave solutions. In particular, contrary to the expectations in [8], there are no such waves in the absence of second-neighbor interactions (discrete Nagumo equation with $d_1 > 0$, $d_2 = 0$).

(a)   (b)
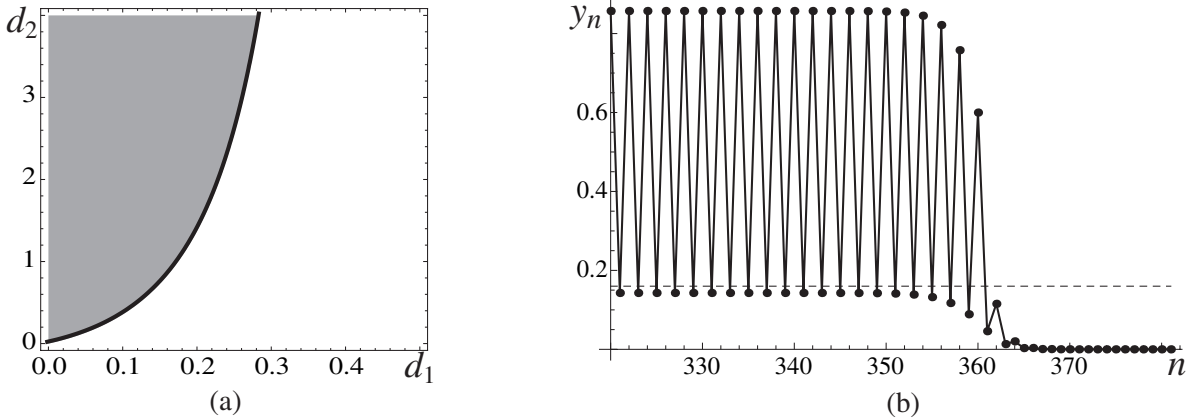
Figure 8. *(a) The shaded region showing the domain of existence of traveling wave solutions with $0 < c < c_{max}(d_1, d_2)$ at positive d_1 and d_2. The black boundary curve is $d_2^*(d_1)$ above which such solutions exist has an asymptote at $d_1 = 0.5$. (b) Snapshots of numerical solution of (2.1), (2.3) (circles) and traveling wave solution (solid line) at $t = 400$ corresponding to $c \approx 0.402$, $d_1 = 0.1$ and $d_2 = 0.5$. Here $a = 0.16$ is marked by the dashed line. The numerical simulations were run with this value of a and the initial condition given by $\mathbf{u}_m(0) = (y_{2m}(0), y_{2m+1}(0)) = (\varphi_1(m - 100), \varphi_2(m - 100))$.*

Fig. 8b shows time snapshots of the traveling wave (solid line) at $d_1 = 0.1$, $d_2 = 0.5$, $a = 0.16$, which corresponds to $c \approx 0.402$, and the results of the numerical simulations (circles) initiated by this wave. The excellent agreement between solutions (difference on the order of 10^{-7}) and velocities (difference on the order of 10^{-9}) suggests stability of this traveling wave. Similar agreement was found with more generic tanh-like initial data and at other values of c.

In the case $d_1 > 0$ and $d_2 < 0$ such that (3.6) holds, a similar analysis yields no traveling wave solutions with $c > 0$ connecting a $p = 2$ equilibrium with $\mathbf{b}^- = (1, 0)$ to zero since in this case the $a(c)$ curves formally obtained from (6.3) always lie below the lower bound in (4.6).

The main results described in this section can be summarized as the follows: our computer-assisted analysis of (6.4) suggests that traveling wave solutions of (2.1), (2.3) connecting a $p = 2$ equilibrium state with $\mathbf{b}^- = (1, 0)$ and zero state exist and are given by (6.1), with the velocity $c > 0$ uniquely determined from (6.3) for given a if

1. $-1/4 < d_1 < 0$, $d_2 \geq 0$, $0 < a < a_+(d_1, d_2)$
2. $-1/4 < d_1 < 0$ and sufficiently small $d_2 < 0$, $0 < a < a_+(d_1, d_2)$
3. $0 < d_1 < 1/2$ and sufficiently large $d_2 > 0$, $2d_1/(1 + 4d_1) < a < a_+(d_1, d_2)$,

where a_+ is given by (6.8). In the last two cases the wave velocity cannot exceed a finite bound that depends on d_1 and d_2. Numerical simulations suggest stability of the traveling waves.

7. The case $p = 3$: some examples. Recall that there are two types of 3-periodic equilibria, (4.7) and (4.9), associated with $\mathbf{b}^- = (1, 0, 0)$ and $\mathbf{b}^- = (1, 1, 0)$, respectively, and that their domain of existence and stability is given by $d_1 + d_2 < 0$, (3.2) and (3.6), with a satisfying (4.8) for $\mathbf{b}^- = (1, 0, 0)$ and (4.10) for $\mathbf{b}^- = (1, 1, 0)$. These inequalities are assumed throughout this section.

In the case $\mathbf{b}^- = (1, 0, 0)$ the periodic equilibrium $\mathbf{u}^-$ behind the moving front is given by (4.7), we have $\hat{h}_1 = -1/(i(s + i0))$, $\hat{h}_2 = \hat{h}_3 = 0$, and the traveling wave solution becomes
(7.1)
$$\begin{pmatrix} \varphi_1(\xi) \\ \varphi_2(\xi) \\ \varphi_3(\xi) \end{pmatrix} = -\frac{1}{2\pi i} \int_\Gamma \frac{e^{is\xi}}{s\Lambda(s,c)} \begin{pmatrix} (1 + 2d_1 + 2d_2 - ics)^2 - d_1^2 - d_2^2 - 2d_1 d_2 \cos(s) \\ e^{-is}(d_2 + d_1 e^{is})^2 + (d_1 + d_2 e^{is})(1 + 2d_1 + 2d_2 - ics) \\ (d_1 + d_2 e^{is})^2 + (d_2 + d_1 e^{is})(1 + 2d_1 + 2d_2 - ics) \end{pmatrix} ds,$$

where

(7.2)
$$\begin{aligned} \Lambda(s,c) = {} & 2d_1^3 + 6d_1(1 + d_2 - ics)(1 + 3d_2 - ics) + 3d_1^2(3 + 4d_2 - 3ics) \\ & + (1 + 2d_2 - ics)(d_2^2 + d_2(4 - 4ics) - (i + cs)^2) \\ & - 2d_1(3d_2 + (d_1 + 3d_2)^2 - 3icd_2 s)\cos(s) - 2d_2^3 \cos(2s). \end{aligned}$$

Setting $\varphi_1(0) = a$ then yields the relation $a = a(c)$ given by

(7.3)
$$a = \frac{1}{2\pi i} \int_\Gamma \frac{d_1^2 + d_2^2 + 2d_1 d_2 \cos(s) - (1 + 2d_1 + 2d_2 - ics)^2}{s\Lambda(s,c)} ds$$

Here a must satisfy (4.8) and the inequalities

(7.4)
$$\varphi_1(\xi) \gtrless a \quad \text{for } \xi \lessgtr 0, \qquad \varphi_2(\xi) < a, \qquad \varphi_3(\xi) < a$$

must also hold. Our parameter study of (7.1), (7.3) showed that a necessary condition for the existence of such traveling waves is that $d_1 < 0$ and $d_2 < 0$: if d_1 and d_2 have different signs, we obtain $a < 0$ for all c, which clearly violates (4.8). In fact, the region of existence is actually smaller, since within the domain defined by $d_1 < 0$, $d_2 < 0$, (3.2) and (3.6) there are neighborhoods near the $d_1 = 0$ and $d_2 = 0$ axes where formal solutions either violate one or more of the assumed inequalities (7.4) or yield negative a for small enough c. The region of existence of $p = 3$ solutions with $\mathbf{b}^- = (1, 0, 0)$ does not appear to overlap with the region of existence of $p = 2$ solutions, where, as we recall, for each $d_1 < 0$ the value of d_2 must be above a sufficiently small negative value to yield a valid solution.

Typical $a(c)$ curves are shown in Fig. 9. One can see that a monotonically decreases and tends to zero as $c \to \infty$ and that the depinning threshold $a(0+)$ decreases as $|d_1|$ or $|d_2|$ become smaller (but remain large enough to ensure existence of admissible solutions for the whole range of velocities). Monotonicity of $a(c)$ curves implies that for given $a > 0$ below the depinning threshold there is a unique velocity $c > 0$ of the traveling wave.

Fig. 10 shows solution snapshots $y_n(t)$ obtained from the shifted traveling wave solution (solid lines) and the numerical simulation (circles) of the system (2.1) with (2.4), (2.5) initiated by the traveling waves with $c = 0.2$ and different values of d_1 and d_2. As in the $p = 2$ case, there is a very good agreement between the analytical and numerical results (though the
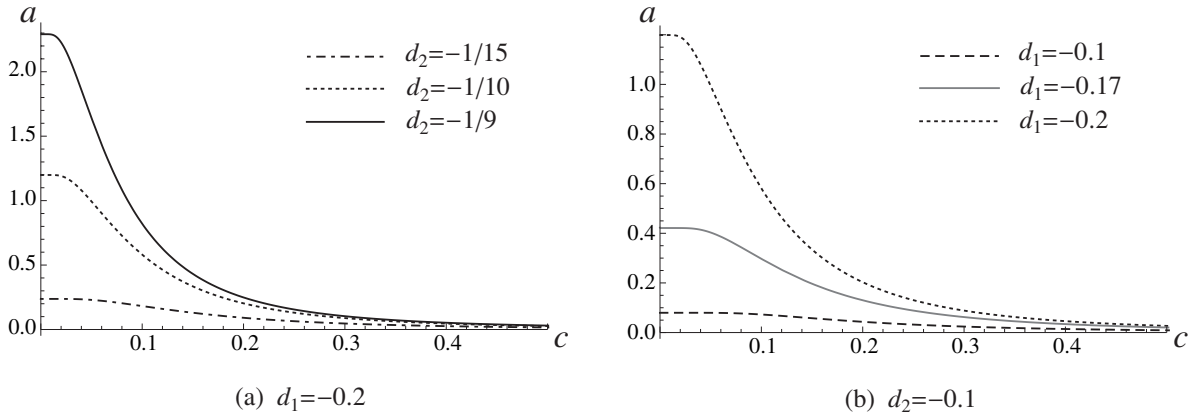
(a) $d_1 = -0.2$ (b) $d_2 = -0.1$

Figure 9. *The relation $a(c)$ at different values of d_1 and d_2*

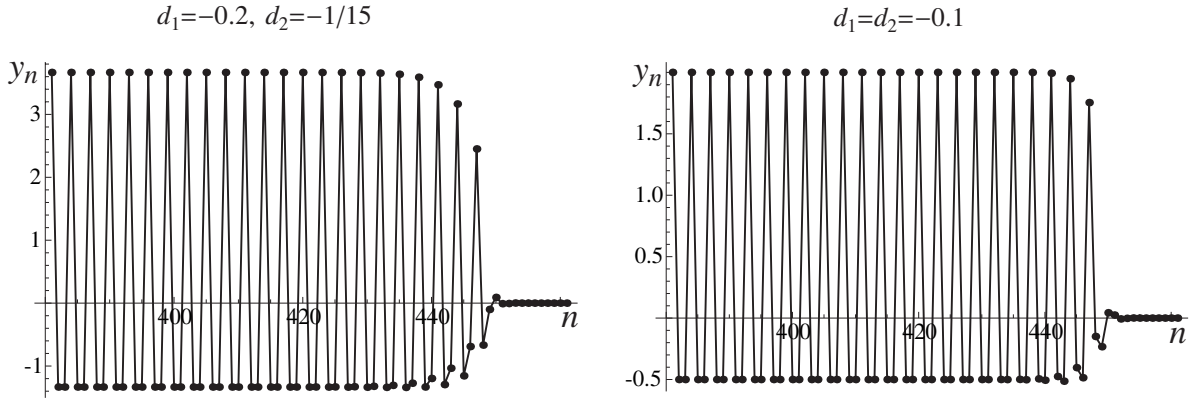$d_1 = -0.2, \; d_2 = -1/15$ $d_1 = d_2 = -0.1$

Figure 10. *Snapshots of numerical solution of* (2.1) *with* (2.4), (2.5) *(circles) and traveling wave solution (lines) at $t = 500$ corresponding to $c = 0.2$ and different values of d_1 and d_2. Here $a \approx 0.091$ at $d_1 = -0.2$, $d_2 = -1/15$ and $a \approx 0.043$ at $d_1 = d_2 = -0.1$. The numerical simulations were run with these values of a and the initial condition given by $\mathbf{u}_m(0) = (y_{2m}(0), y_{2m+1}(0), y_{2m+2}(0)) = (\varphi_1(m-50), \varphi_2(m-50), \varphi_3(m-50))$.*

difference between the solutions is somewhat larger in this case, on the order of 10^{-5}, and the difference between velocities is on the order of 10^{-8}), suggesting stability of the traveling wave solutions, also confirmed by numerical results with more generic tanh-like initial data.

Another type of periodic equilibrium is given by (4.9) and corresponds to $\mathbf{b}^- = (1, 1, 0)$, so we have $\hat{h}_1 = -1/(i(s+i0))$, $\hat{h}_2 = -e^{is\tau}/(i(s+i0))$ (where we set $\xi_1 = 0$ and $\xi_2 = \tau$) and $\hat{h}_3 = 0$. In this case, traveling wave solutions formally obtained by solving (5.3) at $p = 3$ must satisfy $\varphi_1(0) = \varphi_2(\tau) = a$, which can be solved for τ and a. One needs to ensure that a satisfies (4.10) and the inequalities

$$(7.5) \qquad \varphi_1(\xi) \gtrless a \quad \text{for } \xi \lessgtr 0, \qquad \varphi_2(\xi) \gtrless a \quad \text{for } \xi \lessgtr \tau, \qquad \varphi_3(\xi) < a$$

hold. We were not able to find any parameter values inside the region defined by $d_1 + d_2 < 0$, (3.2) and (3.6), where, as we recall, the periodic equilibrium (4.9) exists and is stable for a in

(4.10), for which there exist a traveling wave solution connecting this equilibrium to the zero state that satisfies (4.10) and (7.5). It is possible that such solutions do not exist.

8. The case $p = 4$: some examples.

Traveling waves with $\mathbf{b}^- = (1, 0, 0, 0)$. In this case the periodic equilibrium state $\mathbf{u}^-$ is given by (4.11). Recall that this equilibrium exists and is stable in the domain F in Fig. 4 defined by $d_1 < 0$, $d_1^2 + 2d_1 d_2 + d_2 < 0$, (3.2) and (3.6), with a bounded by (4.12). We have $\hat{h}_1 = -1/(i(s + i0))$, $\hat{h}_2 = \hat{h}_3 = \hat{h}_4 = 0$. Components of the traveling wave solution $\varphi(\xi)$ are then given by

$$\varphi_j(\xi) = \frac{1}{2\pi i} \int_\Gamma \frac{\eta_j(s, c) e^{is\xi}}{s\mathcal{K}(s, c)}, \quad j = 1, 2, 3, 4,$$

where

$$\begin{aligned}
\eta_1(s, c) &= -4d_1^3 + 2d_1^2(-5 - 9d_2 + 5ics + d_2\cos(s)) + (1 + 2d_2 - ics)(-2d_2^2 + d_2(-4 + 4ics) \\
&\quad + (i + cs)^2 + 2d_2^2\cos(s)) + 2d_1(-10d_2^2 + 12id_2(i + cs) + 3(i + cs)^2 + 2d_2^2\cos(s)), \\
\eta_2(s, c) &= -d_1 e^{-is}(d_2^2 + e^{is}(1 + 4d_1 + 3d_1^2 + 6d_2 + 12d_1 d_2 + 10d_2^2 \\
&\quad - 2ic(1 + 2d_1 + 3d_2)s - c^2 s^2) + e^{2is}(d_1^2 + 4d_1 d_2 + d_2(2 + 5d_2 - 2ics))), \\
\eta_3(s, c) &= -(1 + e^{is})(d_1^2 + 2d_1^3 + d_2 + 4d_1 d_2 + 8d_1^2 d_2 + 4d_2^2 + 8d_1 d_2^2 + 2d_2^3 \\
&\quad - ic(2d_2 + (d_1 + 2d_2)^2)s - c^2 d_2 s^2 - 2d_2^3\cos(s)), \\
\eta_4(s, c) &= -d_1(d_1^2 + 2d_2 + 4d_1 d_2 + 5d_2^2 + d_2^2 e^{2is} - 2icd_2 s + e^{is}(1 + 4d_1 + 3d_1^2 + 6d_2 + 12d_1 d_2 \\
&\quad + 10d_2^2 - 2ic(1 + 2d_1 + 3d_2)s - c^2 s^2)),
\end{aligned}$$

and

$$\begin{aligned}
\mathcal{K}(s, c) &= 2d_1^4 + 6d_2^4 - 4d_2^2(1 + 2d_1 + 2d_2 - ics)^2 + (1 + 2d_1 + 2d_2 - ics)^4 \\
&\quad - 4d_1^2(1 + 2d_1 + (3 - i)d_2 - ics)(1 + 2d_1 + (3 + i)d_2 - ics) \\
&\quad - 2(d_1^4 - 4d_2^4 + 2d_2^2(1 + 2d_1 + 2d_2 - ics)^2 \\
&\quad + 4d_1^2 d_2(1 + 2d_1 + 3d_2 - ics))\cos(s) + 2d_2^4\cos(2s).
\end{aligned}$$

Setting $\varphi_1(0) = a$ then yields $a(c)$ relation, where a must satisfy (4.12). For consistency, the solution must satisfy the inequalities

$$(8.1) \qquad \varphi_1(\xi) \gtrless a \quad \text{for } \xi \lessgtr 0, \qquad \varphi_2(\xi) < a, \qquad \varphi_3(\xi) < a, \qquad \varphi_4(\xi) < a.$$

Parameter studies show that these inequalities hold when d_1 is sufficiently small in magnitude for a given d_2 inside the region F in Fig. 4.

Representative $a(c)$ curves are shown in Fig. 11. As in the case of $p = 3$ solution with $\mathbf{b}^- = (1, 0, 0)$, a monotonically decreases and tends to zero as $c \to \infty$, with the depinning threshold $a(0+)$ decreasing with $|d_1|$ and $|d_2|$. Thus we expect a unique wave speed for given $a > 0$ below the depinning threshold. Snapshots of solutions $y_n(t)$ obtained from the shifted traveling wave solution (solid lines) at $c = 0.2$, $d_1 = -0.05$ and two different values of d_2 are shown in Fig. 12, where they are compared to the corresponding snapshots of the

(a) $d_1 = -0.05$ (b) $d_2 = -0.15$
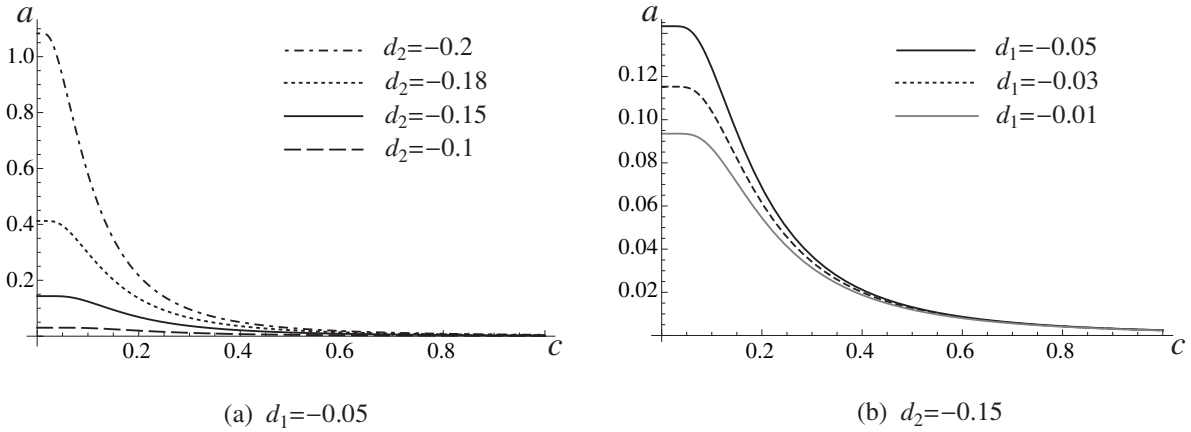
Figure 11. *The relation $a(c)$ at different values of d_1 and d_2.*
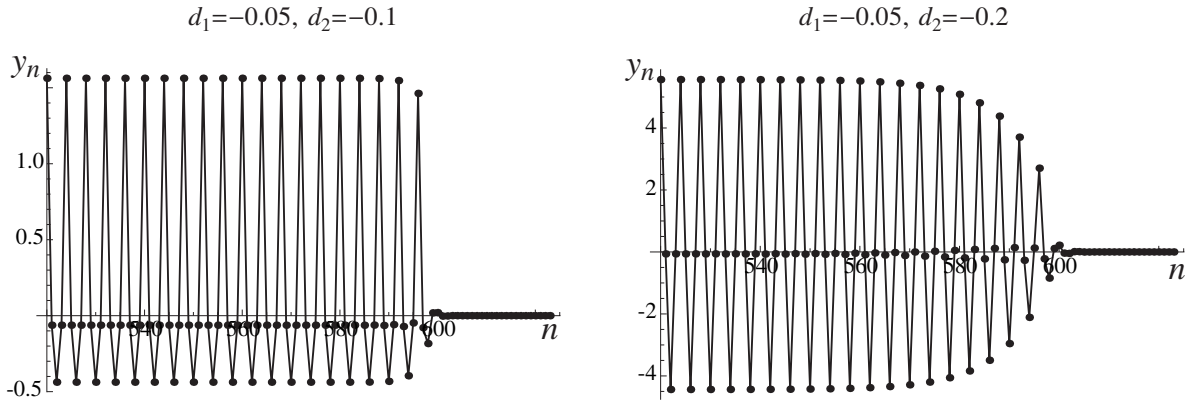
Figure 12. *Snapshots of numerical solution of* (2.1) *with* (2.6), (2.7) *(circles) and traveling wave solution (lines) at $t = 500$ corresponding to $c = 0.2$, $d_1 = -0.05$ and different values of d_2. Here $a \approx 0.02$ at $d_2 = -0.1$ and $a \approx 0.22$ at $d_2 = -0.2$. The numerical simulations were run with these values of a and the initial condition given by $\mathbf{u}_m(0) = (y_{2m}(0), y_{2m+1}(0), y_{2m+2}(0), y_{2m+3}(0)) = (\varphi_1(m - 50), \varphi_2(m - 50), \varphi_3(m - 50), \varphi_4(m - 50))$.*

numerical simulation (circles) of the system (2.1) with (2.6), (2.7) initiated by the traveling waves. The velocity difference is on the order of 10^{-7} in the left and 10^{-9} in the right panel, with similar results for more generic tanh-like initial data, and the maximum absolute value of the difference between the solution snapshots at $t = 500$ is on the order of 10^{-4} and 10^{-5}, respectively, suggesting stability of these traveling waves. But numerical simulations at $d_1 = -0.05$, $d_2 = -0.1$ initiated by a shifted traveling wave with $c = 0.5$ resulted in the numerical solution approaching another wave connecting to a periodic equilibrium with a larger period, indicating instability of the $p = 4$ wave with $\mathbf{b}^- = (1, 0, 0, 0)$ in this case.

Traveling waves with $\mathbf{b}^- = (1, 1, 0, 0)$. Recall that in this case the stable periodic equilibrium state $\mathbf{u}^-$ given by (4.13) exists in the domain defined by $d_1 + 2d_2 < 0$, (3.2), (3.6), with

a bounded by (4.14), and we have

$$\hat{\mathbf{h}}(s) = -\frac{1}{i(s+i0)}(1, e^{-is\tau}, 0, 0),$$

where we set $\xi_1 = 0$ and $\xi_2 = \tau$. The components of $\varphi(\xi)$ can then be found from (5.8) and (5.9); the explicit expressions for their Fourier transforms, which were inverted numerically, are too lengthy in the general case to include here. As described above, we then find τ from $g(\tau) = 0$, where $g(\tau) \equiv \varphi_1(0) - \varphi_2(\tau)$, and then use it to determine $a = \varphi_1(0)$ and hence a relation between c and a. Note that for consistency with our assumptions, a must satisfy (4.14) and the inequalities

$$(8.2) \qquad \varphi_1(\xi) \gtrless a \quad \text{for } \xi \lessgtr 0, \qquad \varphi_2(\xi) \gtrless a \quad \text{for } \xi \lessgtr \tau, \quad \varphi_3(\xi) < a, \qquad \varphi_4(\xi) < a$$

must hold.

In the case $d_1 = 0$ (and hence $d_2 < 0$) the problem decouples, and (5.8), (5.9) simplify to

$$(8.3) \qquad \begin{aligned} \varphi_1(\xi) &= -\frac{1}{2\pi i} \int_\Gamma \frac{1 + 2d_2 - ics}{s\mathcal{L}(s,c)} e^{is\xi} ds \\ \varphi_2(\xi) &= \varphi_1(\xi - \tau) \\ \varphi_3(\xi) &= -\frac{d_2}{\pi i} \int_\Gamma \frac{\cos(s/2)}{s\mathcal{L}(s,c)} e^{is(\xi+1/2)} ds \\ \varphi_4(\xi) &= \varphi_3(\xi - \tau), \end{aligned}$$
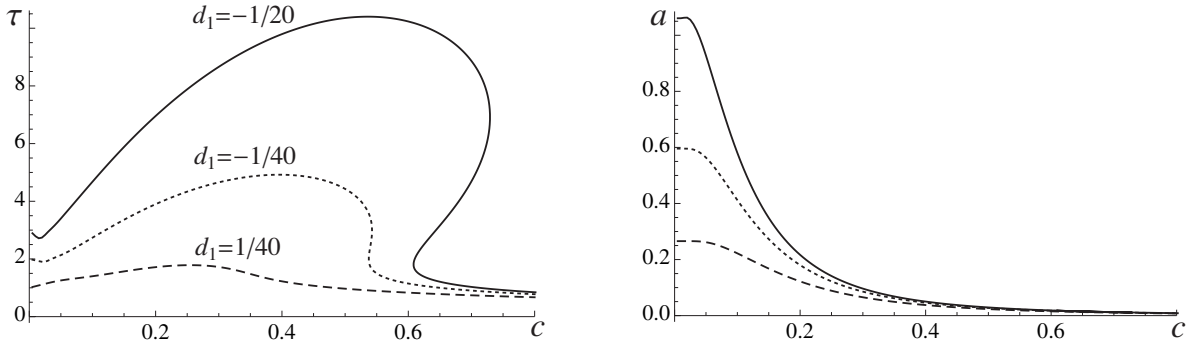
where

$$(8.4) \qquad \mathcal{L}(s,c) = (ics - 2d_2 - 1)^2 - 4d_2^2 \cos^2(s/2).$$

One can see that $(\varphi_1(\xi), \varphi_3(\xi))$ can be obtained from $p = 2$ solution (6.1) by setting $\varphi_2 = \varphi_3$, $d_2 = 0$ and $d_1 = d_2$, and $(\varphi_2(\xi), \varphi_4(\xi))$ is the same solution shifted by τ. These expressions can be evaluated explicitly using the residue theorem as in [31]; see also Appendix A. Note that in this case τ is *arbitrary*, since $\varphi_1(0) = \varphi_2(\tau)$, so that $g(\tau) = 0$ for all τ, but once d_1 becomes nonzero, this is no longer the case. Observe also that at $d_1 = 0$ the condition $\varphi_1(0) = a$ yields the following relation between c and a:

$$(8.5) \qquad a = \frac{1}{2\pi i} \int_\Gamma \frac{ics - 1 - 2d_2}{s\mathcal{L}(s,c)} ds.$$

From the analysis in Sec. 6 and Appendix A we recall that components of $p = 2$ solution at $d_1 < 0$, $d_2 = 0$ are expected to be monotone and satisfy (6.4) for all $c > 0$. This implies that the solution (8.3) at $d_1 = 0$ and $d_2 < 0$ exists for all $c > 0$ and satisfies (8.2). By continuity we expect solutions that satisfy (8.2) to exist for all $c > 0$ at $d_2 < 0$ and sufficiently small nonzero d_1 of either sign.

As an example, consider the case when $d_2 = -0.2$ and d_1 is small enough for such solutions to exist. The corresponding relations $\tau(c)$ and $a(c)$ are shown in Fig. 13. Note that at

Figure 13. *The relations $\tau(c)$ and $a(c)$ at $d_2 = -0.2$ and different values of d_1.*

$d_1 = -1/20$ there is a velocity interval where the relations are multivalued, forming a fold in the graphs (the fold is hard to see for $a(c)$ since the values are very close, but is visible for $\tau(c)$). This implies that in this interval there exist three traveling wave solutions at the same velocity but with different values of τ and slightly different values of a. At $d_1 = -1/40$ the interval where the relations are multivalued also exists but is more narrow, and at $d_1 = 1/40$ the folds disappear, and the relations are single-valued. When $|d_1|$ is large enough, formal solutions may violate one or more of the assumed inequalities (8.2) at some c. For instance, at $d_1 = 0.05$ and $c = 0.5$ the formal solution violates the third inequality in (8.2), while at $d_1 = -1/15$ and $c = 0.2$ the first inequality breaks down.

Running numerical simulations of (2.1) with $\mathbf{A}_k$ given by (2.6), (2.7) and either traveling wave solutions or tanh-like profiles used as the initial conditions, we found that some of the constructed traveling waves appear to be stable. For example, Fig. 14a shows the snapshot of the numerical solution (circles) at $t = 200$ obtained using the traveling wave solution that corresponds to $c = 0.54$, $\tau \approx 2.45$ and $a \approx 0.023$ at $d_1 = -0.025$, $d_2 = -0.2$ and compared to the corresponding snapshots of the traveling wave solution (lines). The difference between the two is very small, less than 10^{-6}. Using shifted tanh-like profiles as initial conditions at the same a, we also found that the numerical solution converges to the same traveling wave, again suggesting its stability. Fig. 14b compares numerical and traveling wave solutions at $d_1 = 0.025$, $d_2 = -0.2$, where $c = 0.8$, $\tau \approx 0.672$ and $a \approx 0.008$, and the agreement is again on the order of 10^{-6}. Meanwhile, numerical simulations at $d_1 = -0.025$, $d_2 = -0.2$ starting with the traveling wave at $c = 0.7$ resulted in a solution that is quite different from the traveling wave. Although initially the numerical solution is close to the traveling wave, at the end of the simulation the second and fourth components moved much slower (with speed $c \approx 0.4$), while only the first and third components moved with velocity $c \approx 0.7$ (see Fig. 15).

Another possibility is that $d_2 \geq 0$ and $d_1 < 0$ are such that the inequalities $d_1 + 2d_2 < 0$, (3.2), (3.6) hold. However, our parameter studies suggest that in this region one always has $a < 0$, so there are no admissible traveling waves.

Traveling waves with $\mathbf{b}^- = (1, 0, 1, 0)$. Recall that in this case the stable periodic equilibrium given by (4.15) is the 4-periodic extension of the 2-periodic equilibrium with $\mathbf{b}^- = (1, 0)$

(a)   (b)
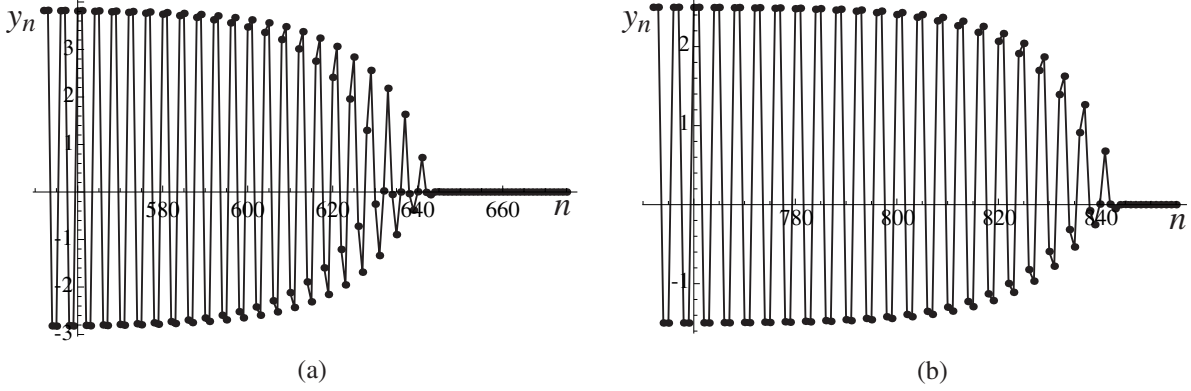
Figure 14. *Snapshots of numerical solution (circles) of* (2.1) *with* (2.6)*,* (2.7) *and the traveling wave solution (lines) at* $t = 200$ *corresponding to (a)* $c = 0.54$*,* $\tau \approx 2.45$ *and* $a \approx 0.023$ *at* $d_1 = -0.025$ *and (b)* $c = 0.8$*,* $\tau \approx 0.672$ *and* $a \approx 0.008$ *at* $d_1 = 0.025$*. Here* $d_2 = -0.2$*, and the numerical simulations were run with these values of* a *and the initial condition given by* $\mathbf{u}_m(0) = (y_{2m}(0), y_{2m+1}(0), y_{2m+2}(0), y_{2m+3}(0)) = (\varphi_1(m - 50), \varphi_2(m - 50), \varphi_3(m - 50), \varphi_4(m - 50))$*.*

and exists in the region defined by $d_1 < 0$, (3.2) and (3.6). Setting $\xi_1 = 0$, $\xi_3 = \tau$, we have

$$\hat{\mathbf{h}}(s) = -\frac{1}{i(s + i0)}(1, 0, e^{-is\tau}, 0).$$

Finding the components of $\varphi(\xi)$ from (5.8) and (5.9), one obtains $g(\tau) \equiv \varphi_1(0) - \varphi_3(\tau)$ of the form

$$g(\tau) = \frac{1}{2\pi} \int_{-\infty}^{\infty} Q(s) \frac{\sin(s(\tau + 1/2))}{s} ds$$

for some function $Q \in L^1(\mathbb{R})$. Thus $g(\tau) = 0$ yields $\tau = -1/2$. Using this one can show that the solution is the 4-periodic extension of the $p = 2$ traveling wave with $\mathbf{b}^- = (1, 0)$ analyzed in Sec. 6 and Appendix A. Specifically, we have $\varphi_1(\xi) = \varphi_1^{(1,0)}(2\xi)$, $\varphi_2(\xi) = \varphi_2^{(1,0)}(2\xi)$, $\varphi_3(\xi) = \varphi_1(\xi + 1/2) = \varphi_1^{(1,0)}(2\xi + 1)$, $\varphi_4(\xi) = \varphi_2(\xi + 1/2) = \varphi_2^{(1,0)}(2\xi + 1)$, where $(\varphi_1^{(1,0)}, \varphi_2^{(1,0)})$ denote the $p = 2$ solution (6.1).

In this section we have analyzed connecting orbits between 4-periodic equilibria that correspond to $\mathbf{b}^+ = (0, 0, 0, 0)$ and $\mathbf{b}^- = (1, 0, 0, 0), (1, 1, 0, 0)$, and $(1, 0, 1, 0)$. In the latter two cases, an additional constraint is obtained that is satisfied for certain values of the shift τ, see, e.g., Fig. 13 when $\mathbf{b}^- = (1, 1, 0, 0)$, $d_2 = -0.2$, and d_1 is varied. In the case of $\mathbf{b}^- = (1, 0, 1, 0)$, a choice for τ is $\tau = -1/2$ in which case the traveling wave solution can be written in terms of shifted versions of the $p = 2$ connecting orbit between $\mathbf{b}^+ = (0, 0)$ and $\mathbf{b}^- = (1, 0)$. Further investigation is warranted for the equilibria considered here, for other equilibria or different combinations of equilibria of periods $p = 2, 3, 4$, and for equilibria of other periods.

9. Concluding remarks. In this paper we have investigated connecting orbits between periodic patterns in a lattice differential equation with competing first and second-neighbor interactions. Using a bilinear bistable nonlinearity we give a relatively complete analysis of periodic patterns of period $p = 2, 3, 4$. Subsequently, we construct traveling wave solutions between the zero steady state and some of these periodic patterns. This system exhibits rich
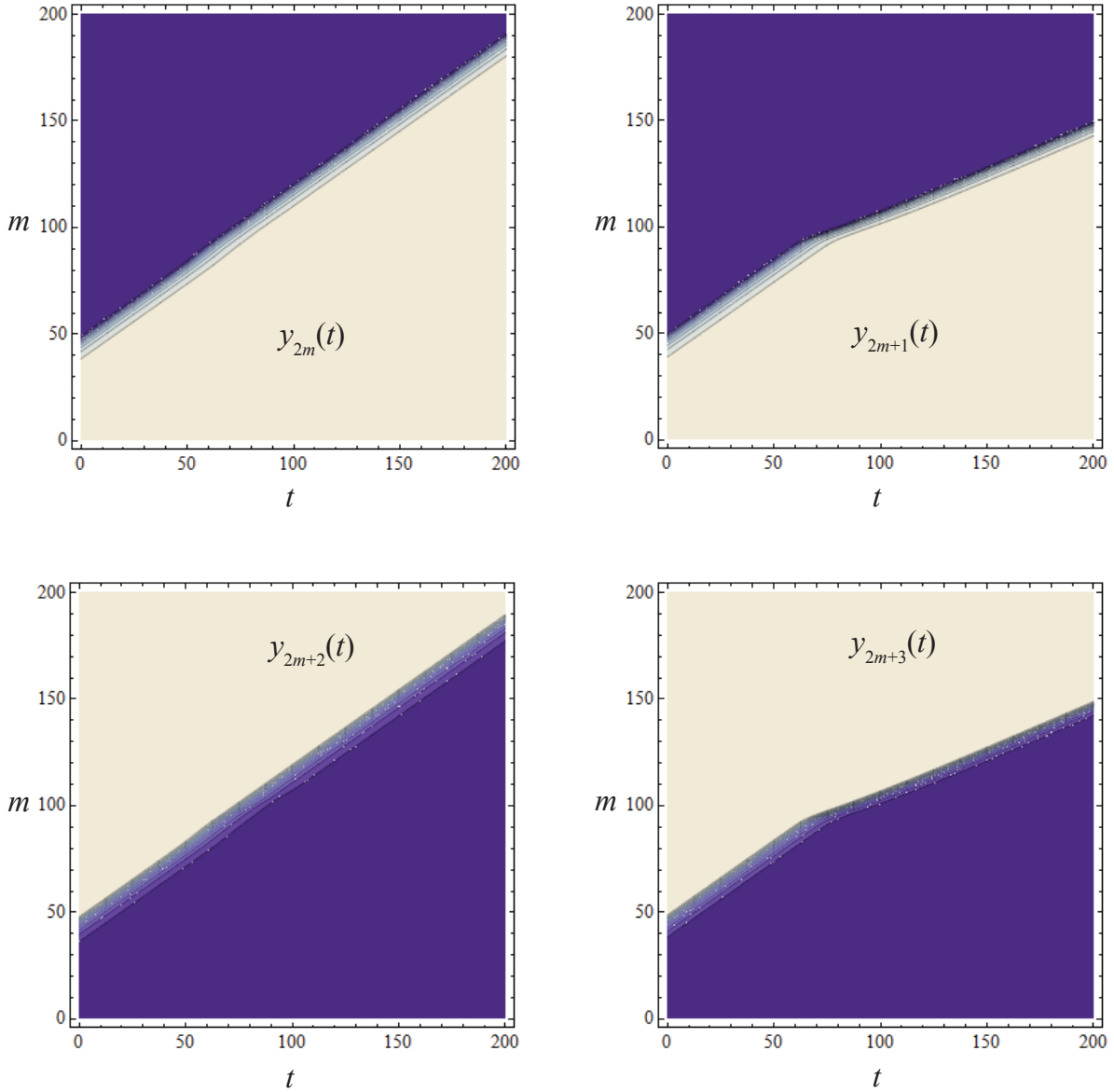
Figure 15. *Contour plots of the solution components $y_{2m}(t)$, $y_{2m+1}(t)$, $y_{2m+2}(t)$ and $y_{2m+3}(t)$ for the simulation initiated by a traveling wave solution with $c = 0.7$, $\tau \approx 0.904$ and $a \approx 0.012$ at $d_1 = -0.025$ and $d_2 = -0.2$. In each plot the darker colors indicate smaller values.*

dynamics including co-existing traveling wave solutions and maximum propagation speed for some patterns. Numerical simulations suggest stability of some of the constructed solutions, while also indicating more complex dynamics in the cases when these solutions are unstable. Interesting future work includes studying existence, stability, and multiplicity of traveling wave solutions between two non-trivial periodic patterns as well as further investigation of cases involving multivalued $\tau(c)$ and $a(c)$ curves like the ones in Fig. 13. In addition, a

more systematic study of the parameter regions where the $a(c)$ relation is monotone can be conducted along the lines of the Melnikov-type approach in Theorem 4.7 of [8].

Appendix. Analysis of solutions at $p = 2$. In this appendix we obtain the explicit solutions for $p = 2$ case and analyze the roots involved in their construction. Here we assume $-1/4 < d_1 < 0$ and (3.6), but the analysis for the case $d_1 > 0$ and (3.6) is similar.

Closing the integration countour Γ in (6.1) by a semiarch at infinity in the upper half-plane for $\xi > 0$ and lower half-plane for $\xi < 0$, and using the Jordan's lemma, we obtain (assuming the generic case when all roots are simple for a given $c > 0$)

(A.1)
$$
\varphi_1(\xi) = \begin{cases} \dfrac{1 + 2d_1}{1 + 4d_1} - \displaystyle\sum_{s \in M^-(c)} \dfrac{ics - 1 - 2d_1 - 4d_2 \sin^2(s/2)}{sL_s(s,c)} e^{is\xi}, & \xi < 0 \\[3mm] \displaystyle\sum_{s \in M^+(c)} \dfrac{ics - 1 - 2d_1 - 4d_2 \sin^2(s/2)}{sL_s(s,c)} e^{is\xi}, & \xi > 0, \end{cases}
$$
$$
\varphi_2(\xi) = \begin{cases} \dfrac{2d_1}{1 + 4d_1} + 2d_1 \displaystyle\sum_{s \in M^-(c)} \dfrac{\cos(s/2)}{sL_s(s,c)} e^{is(\xi + 1/2)}, & \xi < -1/2 \\[3mm] -2d_1 \displaystyle\sum_{s \in M^+(c)} \dfrac{\cos(s/2)}{sL_s(s,c)} e^{is(\xi + 1/2)}, & \xi > -1/2. \end{cases}
$$

The condition $\varphi_1(0) = a$ and the continuity of the solution at $\xi = 0$ then yield

(A.2)
$$
a = \sum_{s \in M^+(c)} \frac{ics - 1 - 2d_1 - 4d_2 \sin^2(s/2)}{sL_s(s,c)} = \frac{1 + 2d_1}{1 + 4d_1} - \sum_{s \in M^-(c)} \frac{ics - 1 - 2d_1 - 4d_2 \sin^2(s/2)}{sL_s(s,c)},
$$

where $L_s \equiv \partial L / \partial s$.

To compute the roots, we first determine the roots of (6.2) at $c = 0$. Since in this case the roots are 2π-periodic, it suffices to consider the roots in the strip $|\mathrm{Re}(s)| \leq \pi$. One can show that at $d_2 \neq 0$ there are four roots in this strip, symmetric about the real and imaginary axes and given by

(A.3)
$$
s = \begin{cases} \pm 2i \mathrm{arccosh} \left\{ \dfrac{1}{4d_2} (\sqrt{4d_2 + (d_1 + 4d_2)^2} \pm d_1) \right\}, & d_2 > 0 \\[3mm] \pm 2i \mathrm{arccosh} \left\{ \dfrac{1}{4d_2} (d_1 \pm \sqrt{4d_2 + (d_1 + 4d_2)^2}) \right\}, & \dfrac{1}{8}(\sqrt{1 + 4d_1} - 1 - 2d_1) \leq d_2 < 0 \end{cases}
$$

and

(A.4)
$$
\begin{aligned} s = &\pm \mathrm{arccos} \left\{ -\frac{1}{4d_2} (1 + 2d_1 + 4d_2 - \sqrt{1 + 4d_1}) \right\} \\ &\pm i \mathrm{arccosh} \left\{ -\frac{1}{4d_2} (1 + 2d_1 + 4d_2 + \sqrt{1 + 4d_1}) \right\} \quad \text{for } d_2 \leq \frac{1}{8}(\sqrt{1 + 4d_1} - 1 - 2d_1). \end{aligned}
$$

In particular, for small nonzero d_2 the roots at $c = 0$ are purely imaginary and given by (A.3). When d_2 tends to zero, the roots with larger modulus tend to infinity, while the ones with smaller modulus tend to $s = \pm 4i \mathrm{arccosh}\{1/(2\sqrt{-d_1})\}$ that were found in [31].

At $c > 0$ $L(s, c) = 0$ is a transcendental equation, and the roots of (6.2) were computed numerically starting with $s + 2\pi n$, where $n \in \mathbb{Z}$ and s are given by (A.3), (A.4), as initial guesses for small c; see, for example, Fig. 16. However, some qualitative conclusions about
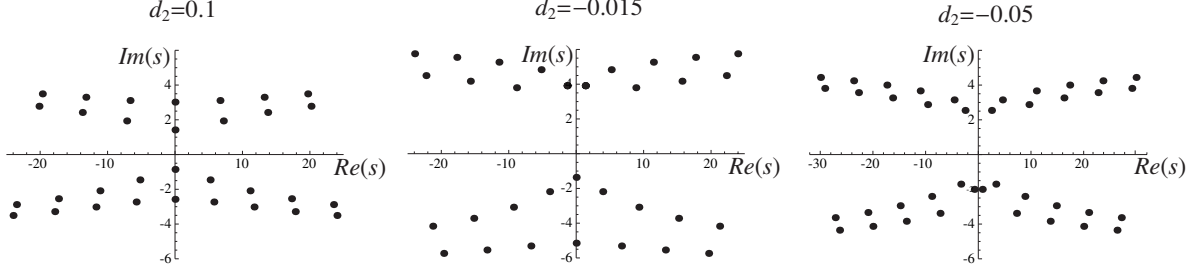
Figure 16. *Roots of* (6.2) *at* $c = 0.1$, $d_1 = -0.2$ *and different* d_2. *Here* $c_- < c < c_+$ *at* $d_2 = -0.015$ *(middle panel) and* $c < c_-$ *at* $d_2 = -0.05$ *(right panel).*

the roots closest to the origin, which determine the structure of the solution profile can be drawn from a simple analysis of $L(s, c) = 0$. In particular, we are interested in the existence of purely imaginary roots $s = i\rho$ because such roots are responsible for creation of boundary layers near the propagating front. Such roots must satisfy either $f_+(\rho) = c\rho$ or $f_-(\rho) = c\rho$, where

$$(A.5) \qquad f_\pm(\rho) = 4d_2 \cosh(\rho/2)^2 \pm 2d_1 \cosh(\rho/2) - 1 - 2d_1 - 4d_2$$

is an even function. At $d_2 > 0$ $f_\pm(\rho)$ tend to infinity as $|\rho| \to \infty$ and are bounded from below by negative values: $f_-(\rho) \geq -1 - 4d_1 < 0$, where we recall (3.2), and $f_+(\rho) \geq f_{min}$, where $f_{min} = -1$ if $d_1 > -4d_2$ and $f_{min} = -1 - (d_1 + 4d_2)^2/(4d_2) \leq -1$ if $d_1 \leq -4d_2$. Thus $f_+(\rho) = c\rho$ or $f_-(\rho) = c\rho$ together yield four purely imaginary roots (two in $\text{Im}(s) > 0$ and two in $\text{Im}(s) < 0$) for any $c \geq 0$. See the the left panel of Fig. 16 ($d_2 = 0.1$) and the top left panel in Fig. 17 for an example. Similar analysis in the limiting case $d_2 = 0$ (where $f_+(\rho) \leq -1$, while $f_-(\rho) \geq -1 - 4d_1 < 0$) yields two purely imaginary roots (one in each half-plane) for c below a certain threshold $c_+(d_1)$, and four purely imaginary roots (one in $\text{Im}(s) > 0$ and three in $\text{Im}(s) < 0$) above the threshold, due to the two complex roots with $\text{Im}(s) < 0$ approaching the imaginary axis and merging at the threshold velocity; see the top right panel ($d_2 = 0$) of Fig. 17. Since these roots have a major contribution to the solution structure, we expect solutions at $d_2 \geq 0$ to have monotone profiles. The situation is different for

$$\frac{1}{8}\left(\sqrt{1 + 4d_1} - 1 - 2d_1\right) < d_2 < 0.$$

In this case $f_\pm(\rho)$ tend to $-\infty$ as $|\rho| \to \infty$, and $f_+(\rho) \leq -1$, while $f_-(\rho)$ has a local minimum $f_-(0) = -1 - 4d_1 < 0$ and maxima

$$f_-\left(\pm 2\text{arccosh}\frac{d_1}{4d_2}\right) = -\frac{4d_2 + (d_1 + 4d_2)^2}{4d_2} > 0.$$

Using this, one can show that $L(s, c) = 0$ has four purely imaginary roots, two in each half-plane, for $0 \leq c < c_-(d_1, d_2)$ but at $c = c_-$ the two imaginary roots with $\text{Im}(s) > 0$ merge and
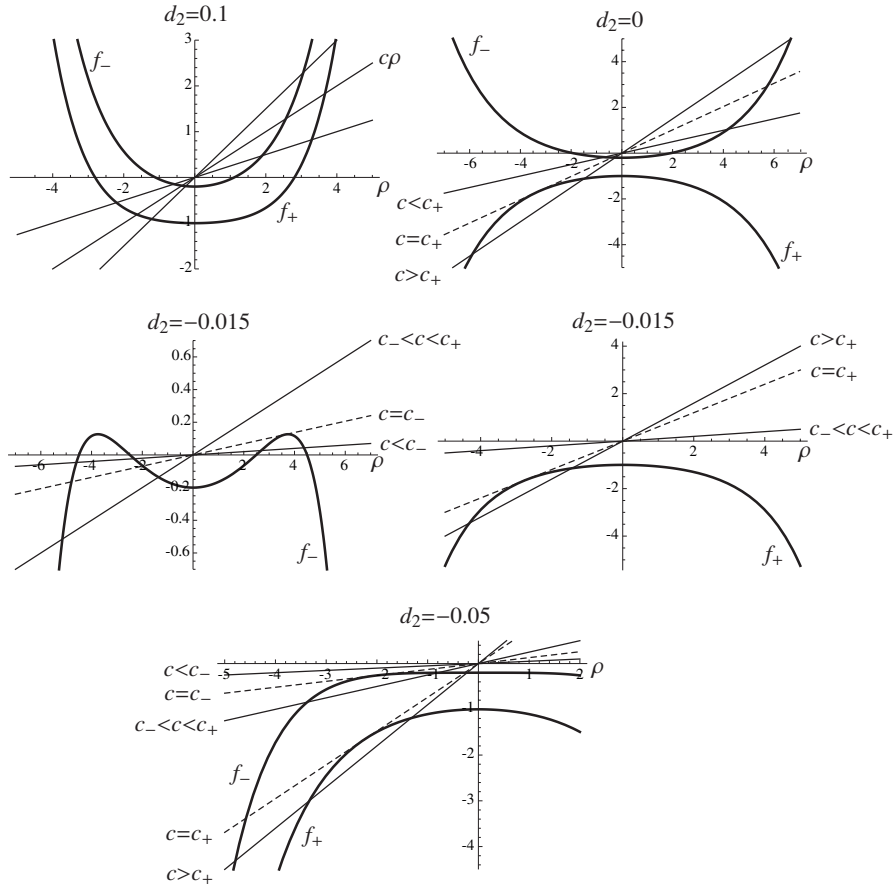
Figure 17. *Graphic representation of solutions of $f_\pm(\rho) = c\rho$ at $d_1 = -0.2$ and different values of d_2 and c. The intersections correspond to the purely imaginary roots of* (6.2)*. Here $c_+ \approx 0.509$ at $d_2 = 0$, $c_- \approx 0.034$, $c_+ \approx 0.599$ at $d_2 = -0.015$, $c_- \approx 0.129$, $c_+ \approx 0.738$ at $d_2 = -0.05$.*

become complex roots $\pm\alpha + i\beta$, $b > 0$, at $c > c_-$; see the middle panel ($d = -0.015$) of Fig. 16 (where $c = 0.1$ is above the threshold $c_- \approx 0.034$) and the middle left panel of Fig. 17. At $c > c_+(d_1, d_2) > c_-$, two additional purely imaginary roots appear in $\mathrm{Im}(s) < 0$ (middle right panel of Fig. 17), due to a pair of complex roots in the lower half-plane merging at $c = c_+$, but no purely imaginary roots with $\mathrm{Im}(s) > 0$ exist for $c > c_-$. At $d_2 = (\sqrt{1 + 4d_1} - 1 - 2d_1)/8$ we have $c_- = 0$. If the complex roots $\pm\alpha + i\beta$, $\alpha > 0$, $\beta > 0$, closest to the origin have a sufficiently large ratio α/β, the (formal) solution profiles for $\varphi_1(\xi)$ and $\varphi_2(\xi)$ become non-monotone at $\xi > 0$ and $\xi > -1/2$, respectively, and may potentially violate at least one of the assumed inequalities $\varphi_1(\xi) < a$ at $\xi > 0$ and $\varphi_2(\xi) < a$ for all ξ. Finally, when

$$d_2 < \frac{1}{8}(\sqrt{1 + 4d_1} - 1 - 2d_1),$$

we have $f_\pm(\rho) \to -\infty$ as $|\rho| \to \infty$, $f_+(\rho) \le -1$, $f_-(\rho) \le -1 - 4d_1 < 0$ if $d_1 \ge 4d_2$ and $f_-(\rho) < -1 - (d_1 + 4d_2)^2/(4d_2) < 0$ if $d_1 < 4d_2$, so there are no purely imaginary roots with $\mathrm{Im}(s) > 0$ at any $c \ge 0$, and no such roots at $\mathrm{Im}(s) < 0$ for $c < c_-(d_1, d_2)$. This is illustrated

in the right panel ($d_2 = -0.05$) of Fig. 16, where, however, two complex roots in $\text{Im}(s) < 0$ are about to merge ($c = 0.1$ is just below $c_- \approx 0.129$). After the roots merge at $c = c_-$, two imaginary roots with $\text{Im}(s) < 0$ appear at $c > c_-$. At $c_+(d_1, d_2) > c_-$ another such bifurcation takes place, resulting in two more purely imaginary roots with $\text{Im}(s) < 0$ at $c > c_+$. Both bifurcations can be seen in the bottom panel ($d_2 = -0.05$) in Fig. 17. As in the previous case, the lack of purely imaginary roots in $\text{Im}(s) > 0$ (in this case for any $c \geq 0$) leads to non-monotonicity of solutions and possible violation of the assumed inequalities.

REFERENCES

[1] P. Bak, *Commensurate phases, incommensurate phases and the devil's staircase*, Rep. Prog. Phys., 45 (1982), pp. 587–629.

[2] P. W. Bates, X. Chen, and A. J. J. Chmaj, *Traveling waves of bistable dynamics on a lattice*, SIAM J. Math. Anal., 35 (2003), pp. 520–546.

[3] J. Bell and C. Cosner, *Threshold behavior and propagation for nonlinear differential-difference systems motivated by modeling myelinated axons*, Quart. Appl. Math., 42 (1984), pp. 1–14.

[4] K. Bhattacharya, *Microstructure of Martensite - Why it Forms and How it Gives Rise to the Shape-Memory Effect*, Oxford University Press, 2003.

[5] O. M. Braun and Y. S. Kivshar, *The Frenkel-Kontorova Model: Concepts, Methods and Applications*, Texts and monographs in physics, Springer-Verlag, Berlin Heidelberg, 2004.

[6] M. Brucal-Hallare and E. S. Van Vleck, *Traveling wavefronts in an antidiffusion lattice nagumo model*, SIAM J. Appl. Dyn. Syst., 10 (2011), pp. 921–959.

[7] J. W. Cahn, S.-N. Chow, and E. S. Van Vleck, *Spatially discrete nonlinear diffusion equations*, Rocky Mountain J. Math., 25 (1995), pp. 87–118.

[8] J. W. Cahn, J. Mallet-Paret, and E. S. Van Vleck, *Traveling wave solutions for systems of ODEs on a two-dimensional spatial lattice*, SIAM J. Appl. Math., 59 (1999), pp. 455–493.

[9] V. Celli and N. Flytzanis, *Motion of a screw dislocation in a crystal*, J. Appl. Phys., 41 (1970), pp. 4443–4447.

[10] X. Chen, J.-S. Guo, and C.-C. Wu, *Traveling waves in discrete periodic media for bistable dynamics*, Arch. Ration. Mech. Anal., 189 (2008), pp. 189–236.

[11] R. Coutinho and B. Fernandez, *Fronts between periodic patterns for bistable recursions on lattices*, J. Dyn. Diff. Eq., 25 (2013), pp. 17–31.

[12] S. V. Dmitriev, K. Abe, and T. Shigenari, *Domain wall solutions for EHM model of crystal: structures with period multiple of four*, Phys. D, 147 (2000), pp. 122–134.

[13] C. E. Elmer and E. S. Van Vleck, *Spatially discrete fitzhugh-nagumo equations*, SIAM J. Appl. Math., 65 (2005), pp. 1153–1174.

[14] B. Ermentrout, *Neural networks as spatio-temporal pattern-forming systems*, Rep. Prog. Phys., 61 (1998), pp. 353–430.

[15] T. Erneux and G. Nicolis, *Propagating waves in discrete bistable reaction-diffusion systems*, Phys. D, 67 (1993), pp. 237–244.

[16] G. Fáth, *Propagation failure of traveling waves in discrete bistable medium*, Phys. D, 116 (1998), pp. 176–190.

[17] A. F. Filippov, *Differential Equations with Discontinuous Righthand Sides*, vol. 18 of Mathematics and its Applications (Soviet Series), Kluwer Academic Publishers Group, Dordrecht, 1988.

[18] W. Hudson and B. Zinner, *Existence of traveling waves for a generalized discrete Fisher's equation*, Comm. Appl. Nonlinear Anal., 1 (1994), pp. 23–46.

[19] H. J. Hupkes and E. S. Van Vleck, *Negative diffusion and traveling waves in high dimensional lattice systems*, SIAM J. Math. Anal., 45 (2013), pp. 1068–1135.

[20] T. Janssen and A. Janner, *Incommensurability in crystals*, Adv. Phys., 36 (1987), pp. 519–624.

[21] J. P. Keener, *Propagation and its failure in coupled systems of discrete excitable cells*, SIAM J. Appl. Math., 47 (1987), pp. 556–572.

[22] P. G. Kevrekidis, *Non-linear waves in lattices: past, present, future*, IMA J. Appl. Math., 76 (2011), pp. 1–35.

[23] J. Mallet-Paret, *Traveling waves in spatially discrete dynamical systems of diffusive type*, in Dynamical systems, vol. 1822 of Lecture Notes in Math., Springer, Berlin, 2003, pp. 231–298.

[24] S. Marianer and A. R. Bishop, *Frenkel-Kontorova model with nonconvex-interparticle interactions and strain gradients*, Phys. Rev. B, 37 (1988), pp. 9893–9896.

[25] S. Marianer and L. M. Floria, *Application of the method of effective potentials to a model for twinning in elastic materials*, Phys. Rev. B, 38 (1988), pp. 12054–12057.

[26] J. P. Sethna, *Statistical Mechanics: Entropy, Order Parameters, and Complexity*, vol. 14, Oxford University Press Oxford, 2006.

[27] L. I. Slepyan, *Models and Phenomena in Fracture Mechanics*, Springer-Verlag, New York, 2002.

[28] A. K. Tagantsev, L. E. Cross, and J. Fousek, *Domains in Ferroic Crystals and Thin Films*, Springer, 2010.

[29] L. Truskinovsky and A. Vainchtein, *Quasicontinuum modeling of short-wave instabilities in crystal lattices*, Phil. Mag., 85 (2005), pp. 4055–4065.

[30] ———, *Dynamics of martensitic phase boundaries: discreteness, dissipation and inertia*, Cont. Mech. Thermodyn., 20 (2008), pp. 97–122.

[31] A. Vainchtein and E. S. Van Vleck, *Nucleation and propagation of phase mixtures in a bistable chain*, Phys. Rev. B, 79 (2009), p. 144123.

[32] E. S. Van Vleck and A. Zhang, *Competing interactions and traveling waves in lattice differential equations*, submitted, (2014).